Evaluating the role of tectonics, eustasy, and climate on the Maastrichtian-Danian transgression in the Magallanes-Austral Basin (Chilean Patagonia)

Huber A. Rivera[1, 2, *], Jacobus P. Le Roux[1], Marcelo Farías[1], Néstor M. Gutiérrez[1], Alejandro Sánchez[3], Sylvia Palma-Heldt[4], Lissett Celle[1]

[1]Departamento de Geología, FCFM, Universidad de Chile, Plaza Ercilla 803, Santiago, Chile

[2]Univ. Grenoble Alpes, Univ. Savoie Mont Blanc, CNRS, IRD, IFSTTAR, ISTerre, 38000 Grenoble, France

[3]Departamento de Ingeniería en Minas, Universidad de Santiago de Chile, Av. O'Higgins 3363, Estación Central, Santiago, Chile

[4]Departamento de Ciencias de la Tierra, Universidad de Concepción, Barrio Universitario S/N°, Concepción, Chile

***Corresponding author:** riverarh@univ-grenoble-alpes.fr; huber.rivera@ug.uchile.cl

ABSTRACT

The Maastrichtian-Danian transgression was the first and most extended Atlantic-derived marine incursion in Patagonia, and the detailed study of its stratigraphic record and causative mechanism in the Magallanes-Austral Basin reveals the interplay of sedimentation, tectonism, and base-level changes. This contributes to our understanding of the foreland basin dynamics. We present a multi-faceted approach including sedimentology, palynology, sequence stratigraphy, and geochronology, to evaluate the role of climate, tectonics, and eustasy on the transgression. Two stratigraphic sequences are recognized: (1) from the late Campanian to Maastrichtian, when a normal regression occurred that shifted shelf and upper slope deposits (Fuentes Formation) to shoreface and deltaic environments (Rocallosa-Dorotea Formations) favoured by high erosion rates in the fold-thrust belt and a sea-level drop during a prevailing cool, rainy, and humid climate; (2) from late Maastrichtian to Paleocene when the transgression took place, manifested by estuarine deposits (upper Dorotea Formation) in an incised valley system and by deep-water turbidites (Chorrillo Chico Formation and Cabo Naríz beds). The development of the stratigraphic

sequences was mainly tectonic-driven where the interplay of flexural loading and sediment supply sourced from the uplifted Patagonian Andes shape the evolution of the accommodation space. This study highlights the significance of a major thrusting event at *ca*. 67 Ma that generated flexural subsidence causing the transgression, as well as two phases of Patagonian orogenic building and long-term detritus input from the Southern Patagonian Batholith, mafic Rocas Verdes Basin remnants, and Andean metamorphic terranes exposed in the hinterland. Moreover, point-out the importance of the preceding basin configuration to the formation whether of subaerial unconformities or correlative conformities.

Keywords: Incised valley; Transgression; Patagonian Andes; Cretaceous paleoclimate; sequence stratigraphy.

1. INTRODUCTION

The study and understanding of transgressions have become of vital importance in almost all basins that are of interest for petroleum exploration. In addition, transgressions have significant implications in active foreland basins since they not only reflect the interplay of dynamic and flexural subsidence in deepening the basin (e.g., Mitrovica *et al*., 1989; Sinclair *et al*., 1998) but also allow a better understanding of the balance of tectonic loading-unloading, sedimentation, and sea-level changes within their complex and dynamic evolution (e.g., Catuneanu, 2004; Yang & Miall, 2008; Rodazz *et al*., 2010).

In Patagonia, the Maastrichtian-Danian transgression is considered to have been the first, deep and extended Atlantic marine ingression (Malumián & Náñez, 2011). Contrary to most other Cenozoic transgressions, the first Atlantic transgression was not related to relative climatic optima and appears to have been linked to significant cooling conditions, accompanied by a gradual sea-level decline between the Maastrichtian and Danian (Barrera & Savin, 1999; Haq, 2014; Huber,

2018), which raises interesting questions about the role of eustatic versus tectonic processes during the transgression.

To date, the best indicator of this transgression lies in the foraminifera assemblage recorded in all the Patagonian basins except for the Península Valdes and Rawson Basins (Náñez & Malumián, 2009; Malumián & Náñez, 2011). A good sedimentological record being present only in the northernmost basins (Aguirre-Urreta *et al*., 2011 and references therein). The stratigraphic record of this transgression is unknown throughout the Magallanes-Austral Basin because (1) the K-Pg boundary has been hardly recognized (Charrier & Lahsen, 1969; Malumián & Caramés, 1997; Malumián & Náñez, 2011), and (2) there is a lack of sequence-stratigraphic and sedimentological studies on the K-Pg transition. On the other hand, the continuous history of marine sedimentation in the Magallanes-Austral Basin (Fig. 1a) since its formation, imposes an even greater complexity to decipher the relative control between the processes that intervene in the transgression.

The aim of our work is to broaden current knowledge of the stratigraphic record of the first Atlantic transgression and its causative mechanism in the Magallanes-Austral Basin (Fig. 1a) by a multidisciplinary approach, including sedimentological, sequence stratigraphic, palynological, and geochronological studies. Our study examines to what extent the climate, eustasy and tectonics controlled the marine incursion and provides a sequence stratigraphic framework that facilitates the understanding of the juxtaposition, evolution, and inter-basin correlation of the depositional units (from Campanian-Maastrichtian to Paleocene). In addition, the results of this study allow us to constrain the timing of the latest Cretaceous-early Cenozoic tectonic events and establish an accurate delineation of sea-level changes at the K-Pg transition, which have significant

implications for our understanding of the palaeofaunistic and palaeofloristic interchange dynamics between South America and the Antarctic Peninsula.

2. TECTONIC AND STRATIGRAPHIC SETTING

2.1 Stratigraphic synthesis of the study area

Our study encompasses the uppermost Fuentes, Rocallosa-Dorotea, and Chorrillo Chico Formations (Fig. 1b). The locations of stratigraphic sections are primarily on the Brunswick Peninsula, the northern coast of the Skyring Sound and Riesco Island, belonging to the Magallanes Province (MP; Fig. 2); the Cerro Pelario, Demaistre area, and the southern extension of Sierra Dorotea, belonging to the Última Esperanza Province (UEP; Fig. 2). Additionally, we present petrological data of the Cabo Naríz strata (equivalent to the Chorrillo Chico Formation) studied previously by Sánchez *et al*. (2010) in the west coast of Tierra del Fuego (Fig. 1a). This strategic distribution of stratigraphic sections (Table 1; Fig. 2) allows us to study in greater detail the facies changes and depositional evolution along the axis of the basin.

The K-Pg stratigraphic nomenclature between Argentina and Chile (and within Chile itself) is particularly confusing as many units are referred to by different names (Fig. 1b). Moreover, the Maastrichtian-Danian transgression and subsequent regressive deposits have been unevenly studied on both sides of the international boundary. In the Río Turbio area (Argentina) (Fig. 1a), the massive, glauconitic sandstones with intercalations of mudstones, and conglomerates of the Monte Chico Formation (Maastrichtian-Danian; Fig. 1b) followed by the fine-to-coarse-grained sandstone- and conglomerate-bearing coal seams of the Cerro Dorotea Formation (Danian-Selandian; Fig. 1b) are often thought to represent a transgressive-regressive (T-R) cycle (Malumián & Caramés, 1997; Álvarez *et al*., 2006; Mpodozis *et al*., 2011; Fosdick *et al*., 2015)

and it can only be assumed (indirectly) that the Maastrichtian-Danian Atlantic transgression is equivalent to the T hemicycle. In any case, such a cycle has not been yet identified in the equivalent deltaic Dorotea Formation (as referred to in the Chilean UEP) nor in the Chilean MP (Fig. 1b, 2), where it is represented by a succession of fine- to coarse-grained, argillaceous, glauconitic sandstones of the Rocallosa Formation (late Campanian-Danian) (Charrier & Lahsen, 1969; Castelli *et al*., 1992; Álvarez *et al*., 2006; Mpodozis *et al*., 2011). Moreover, the stratigraphic relationships of the Rocallosa Formation with the overlying, deep-water shales, siltstones, and clay-rich glauconitic sandstones of the Chorrillo Chico Formation (Paleocene) and the underlying, shale-dominated Fuentes Formation (Campanian) (Charrier & Lahsen, 1969; this study) are unknown.

2.2 Tectonic framework

The Magallanes-Austral Basin (Fig. 1a) is a retroarc foreland basin (Fildani *et al*., 2008; Fosdick *et al*., 2011) oriented subparallel to the Southern Patagonian Batholith (Jurassic to Neogene; Hervé *et al*., 2007) which intruded low-grade, metasedimentary components of the Andean metamorphic complexes (late Devonian to Permian; Hervé *et al*., 2003). The fold-and-thrust belt bounding the Magallanes-Austral Basin to the west (Fig. 1a), represents the primary source of sediments to the basin and exposes remnants of the Late Jurassic-Early Cretaceous (154-100 Ma) siliceous, argillaceous, and ophiolitic rocks of the extensional Rocas Verdes Basin (Dalziel, 1981; Calderón *et al*., 2007; Fildani *et al*., 2008), and clastic deposits of the exhumed foreland basin strata (Fig. 1a, b).

At least 3 tectonic loading pulses have been documented during the Cretaceous-Paleocene in the basin. The Late Cretaceous (92-100 Ma) pulse was responsible for the closure of the extensional Rocas Verdes Basin and initial turbidite filling of the early Magallanes-Austral Basin

(Calderón *et al*., 2007; Fildani *et al*., 2008; Romans *et al*., 2010; Fosdick *et al*., 2011). Another major pulse of contractional deformation is inferred (86-80 Ma) by the incorporation of Upper Jurassic igneous units, mafic, and metamorphic source terrane material in the hinterland (Romans *et al*., 2010; McAtamney *et al*., 2011). Finally, a loosely constrained (74-27 Ma) deformational pulse (Tenerife thrust of Fosdick *et al*., 2011) that incorporated Upper Jurassic felsic to intermediate (meta-)volcanic rocks, and Upper Cretaceous foredeep deposits into the fold-and-thrust belt occurred, to which is ascribed the progradation and shoaling of the depositional system (Schwartz & Graham, 2015; Schwartz *et al*., 2017; Gutiérrez *et al*., 2017).

3. FACIES ASSOCIATIONS AND PALAEOENVIRONMENTS

A total of 9 stratigraphic columns (some composite) (Table 1; Fig. 3) were measured bed-by-bed at a cm-dm scale (totaling ~1500 m), using a Jacob staff and measuring tape on the best available exposures. Palaeocurrent directions were measured, including planar and trough cross-lamination, tool marks, turboglyphs, and ripple marks. Nine major facies associations (FA) were recognized and some sub-facies associations have been described as well. Table 2 presents a detailed description of the overall facies identified.

3.1 Facies association 1 (FA1): Outer shelf, low-density turbidites

The FA1 occurs in the upper part of the Fuentes Formation in Section BH (Table 1; Fig. 2c) and consists of thin intercalations of laminated shales (Fh), and massive to vaguely laminated siltstones (Slm) and sandstones (Sm). Some tabular mudstone (Fm) intervals are also present, which reach up to tens of meters in thickness (Fig. 5a). Occasionally, sedimentation units grade internally in cycles typically about 15 cm thick. Slump structures, tool marks at the bases of Sm facies, and laterally continuous contorted marlstone beds were also observed. The bioturbation

index (BI) varies with each facies, in the Fh and Fm facies being 0 – 3. The former is characterized by abundant *Stelloglyphus llicoensis* (Fig. 6f), *Chondrites* isp., *Phycosiphon incertum* ?, *Planolites* isp., and rare *Rhizocorallium* isp., and *Bergaueria* isp., and the latter by *Phycodes* isp. (Fig. 6a), *Palaeophycos* isp., *Cladichnus* cf. *fischeri* (Fig. 6e) and *Phoebichnus bosoensis* (Fig. 6d); The Sm and Slm facies are more bioturbated, with a BI of 2 – 4, and contain *Thalassinoides* isp., *Cylindrichnus* isp., and undetermined trace fossils.

The fine-grained nature of the overall facies association and degree of bioturbation related to the Zoophycos ichnofacies suggest a very low energy and open marine environment below the storm-wave base. The thick mudstone facies (Fm) and internally graded units (Fh and Sm) reflect settling of hemipelagic mud and deposition of mud-rich, low density turbidity currents (Covault *et al*., 2009) in an outer shelf setting, as suggested by the slump and contorted structures, and the abundant presence of *Stelloglyphus llicoensis* commonly found in this kind of environment (Le Roux *et al*., 2008).

3.2 Facies association 2 (FA2): Offshore transition

FA2 is characterized by tabular mudrocks (Fm and Fh) that rapidly grade upward into well-stratified siltstones (Slm and Slh), massive, fine-grained sandstones (Sm) with tool marks at the base, fine-to-medium-grained sandstones with hummocky cross-stratification (Shcs) and planar, low-angle cross lamination (Spl) commonly showing some wave ripple-lamination (Sw) slightly contorted at the tops. The FA2 occurs throughout the Rocallosa and Dorotea Formations (Fig. 3a, b) and is generally capped by the FA3 in a gradual contact. It is represented by a 10 – 70 m thick succession. Laterally continuous carbonate concretions are typically abundant, and in some cases form isolated bodies of up to 3 m long. The glauconite content is generally low in the mudstone but moderate in the sandstone facies. The BI is 1 – 4 characterized by *Palaeophycus* isp., *Planolites*

isp., *Chondrites* isp., *Zoophycos* isp., *Thalassinoides* isp., and *Teichichnus* isp. (Fig. 6h), with trace fossils confined to the bedding planes.

The relative abundance of silt and sand grain sizes, as well as storm- (Shcs) and wave-generated (Sw) structures indicates that the depositional setting was shallower than that of the FA1, above the storm wave base and close to the fair-weather wave base (Rossi & Steel, 2016), but the trace fossil assemblage still indicates a fully marine environment. The HCS sandstone beds and Spl facies suggest the influence of strong oscillatory or combined flows, whereas the associated symmetrical ripples (Sw) indicate the waning phases of storm-related events (Dott & Bourgeois, 1982). However, the slightly contorted wave ripple tops can be explained by the action of subsequent surge flows that developed high shear stress and liquefied the previously deposited beds. They could also have resulted from gravity-driven instability acting on unconsolidated water-saturated sediments (McDonald, 1986; Myrow *et al*., 2002). This facies association represents sedimentation in a phase of progradation from an offshore to lower shoreface environment.

3.3 Facies association 3 (FA3): Lower shoreface

The FA3, representing a typical lower shoreface, is present in all sections where the Rocallosa and Dorotea formations were studied (Table 1; Fig. 3a, b). It comprises a crudely coarsening- and thickening-upward arrangement formed by packages of up to 70 m thick. The FA3 (Fig. 4g) consists of wispy, and planar laminated siltstones (Slh) (Fig. 4h), vaguely stratified, massive siltstones (Slm), well-stratified and massive, bioturbated, fine-grained sandstones (Sm) internally showing crude normally graded cycles up to 10 cm thick, and finally HCS sandstone packages (Shcs) with pebbly sandstones on the erosive bases. The latter are commonly associated with wave rippled beds (Sw). Glauconite is present throughout and the BI is 1 – 4, being

characterized by *Zoophycos* isp., *Chondrites* isp., *Planolites* isp., *Teichichnus* isp. (Fig. 6j), and *Palaeophycus* isp.

The characteristic good stratification, HCS, symmetrical ripples, wispy lamination and abundant trace fossil assemblage of Cruziana ichnofacies suggest a wave-dominated open marine environment (Buatois & Mángano, 2011) where sedimentation mechanisms were similar to FA2. According to its stratigraphic position and the interplay with adjacent facies associations it has been interpreted as representing lower shoreface deposits.

3.4 Facies association 4 (FA4): Mid-to-upper shoreface/ beach-foreshore

This facies association is divided into 2 sub-facies: FA4a and FA4b (the latter being rarely present). The FA4 occurs mainly in the Dorotea Formation (Fig. 4e) and subordinately in the upper part of the Rocallosa Formation (sections PE and PP; Table 1 and Fig. 3b), transitionally overlying FA3 and FA6a facies arranged in coarsening-upward sequences ranging from 1 to 7 m thick. The FA4a is composed mostly of well-sorted, fine-to-coarse-grained sandstones showing amalgamated beds with hummocky- and swaley cross-stratification (HCS) (Shcs) (Fig. 4f), trough cross-bedding (St; sometimes diffuse), and planar- and low-angle cross-stratification (Spl). Locally, pebbly sandstones or massive, fine-grained sandstones (Sm), and planar laminated siltstones (Slh) can be intercalated. Abundant carbonaceous material, shelly hash, coarse-grained and conglomeratic lenses and scour-and-fill structures are present; the scours are mantled by quartz, andesitic, and reworked glauconite grains. In section PE (Table 1; Fig. 2) rare angular to sub-angular pebbles and cobbles (up to 7 cm in diameter) composed of glauconite, quartz, and lithic fragments (Fig. 9a) are dispersed in the sandstones beds. The FA4b comprises 1 m thick, well-sorted, medium-grained sandstone with low-angle cross-lamination and upper plane lamination (Spl). Bioturbation is low to absent (BI 0 – 1).

The presence of St and Spl facies and the well-sorted nature of the sediments reflect accumulation in longshore runnels in the surf and breaker zone where there is continuous wave reworking in a high-energy environment above the fair-weather wave base. Amalgamated HCS and SCS suggest the action of large-scale oscillatory currents related to storm waves combined with unidirectional currents (Dumas & Arnott, 2006), while the transition of hummock- to swale-dominated units reflect a basin-ward advance of the shoreline. These strong unidirectional currents are indicated the shelly hash, organic detritus, coarse-grained lenses, and scours associated with offshore-directed rip currents during storm events. The FA4 is therefore interpreted as a mid-to-upper shoreface environment. However, the angular to sub-angular pebbles and cobbles dispersed in scoured coarse-grained sandstones (in section PE) can be interpreted as a foreshore-beach environment where low-angle cross-lamination, and upper flow regime planar lamination record swash processes caused by the breaking waves in a likely reflective beach.

3.5 Facies association 5 (FA5): Prodelta

This facies association is present only in the Dorotea Formation in section SD (Table 1; Fig. 2). FA5 (Fig. 4a) is dominated by 1 – 6 m thick, laminated shales (Fh) and massive mudstones (Fm) intercalated with sharp-based, tabular, massive siltstones (Slm) and very fine-grained sandstone (Sm) beds up to 50 cm thick. In a few cases, the muddy deposits are punctuated by 60 cm thick, tabular, very fine-grained sandstones with HCS (Shcs). FA5 gradually coarsens upwards and grades into FA6. The BI ranges from 0 – 2 (*Chondrites* isp., *Zoophycus* isp., *Teichichnus* isp., *Planolites* isp., and *Taenidium* isp.) and is concentrated in the lower mudrock intervals.

The fine grain sizes (Fm, Fh), planar lamination (Fh) and degree of bioturbation suggest a low energy setting where settling and vertical accretion of suspended sediments took place in an open marine environment. The larger grain size facies (Slm, Sm, and Shcs) reflect deposition

because of rapid fallout sands triggered by hyperpycnal density underflows or wave-induced storm currents (Bhattacharya, 2010). The overall facies association with coarsening-upward trend is interpreted as the distal reaches of prograding deltaic lobes (Rossi & Steel, 2016) and the lack of bioturbation in the upper parts of the succession suggests high sedimentation rates and salinity stress (MacEachern *et al*., 2005) during high river discharges, consistent with a prodelta environment.

3.6 Facies association 6 (FA6): Delta front / wave-modified distal delta front

Three sub-facies associations (FA6a, b, c) are grouped here which form the clinothems of the Dorotea Formation (Fig. 4a, b), well represented in section SD (Table 1; Fig. 2). The FA6 generally comprises a coarsening- and thickening-upward arrangement, characterized by packages ranging from 20 – 40 m thick, which are associated vertically and laterally with FA4 and FA5. The FA6a is composed of lower planar-laminated, fine-to-medium-grained sandstones (Spl), trough cross-laminated beds (St), and massive, very fine-grained sandstone (Sm). Some intercalations of massive siltstone beds (Slm), coarse-grained lenses, scour surfaces (filled with HCS or Spl facies; Fig. 4c) and carbonaceous plant debris can be observed. Some *Turritela* sp. and fragmented shell can be present. Bioturbation (BI of 1 – 4) is mainly restricted to the Sm facies and consists of *Thalassinoides* isp., *Chondrites* isp., *Taenidium* isp., *Asterosoma* isp., and *Ophiomorpha* isp. The FA6b consists of 2 – 4m thick packages of interbedded, amalgamated, massive, fine-to medium-grained sandstones (Sm), and medium-grained sandstones with dune-scale (sets of ~10 m wavelength and 1 m height) trough cross-bedding (St) (Fig. 4b) frequently associated with scour-and-fill structures filled with coarse to gritty sandstones. Bioturbation is generally low (BI of 1 –2) and represented by *Macaronichnus* isp. (Fig. 6i), *Planolites* isp., and *Diplocraterion* ? isp. The FA6c is arranged in fining-upward sequences of up to 8 m thick, which

comprise normally graded, very coarse to (upper) medium-grained sandstones (Sm) with scoured bases and rip-up clasts, followed by medium-grained, planar or trough cross-bedded sandstones (Spa, St) with some muddy partings. Bioturbation (BI of 0 – 1) is very limited and restricted to *Schaubcylindrichnus* isp. (Fig. 6k).

The cross-bedded and massive sandstones (St, Sm) in the FA6a likely represent deposition under rapidly decelerating unidirectional flows in sandy delta fronts (Bhattacharya, 2010). The river influence is expressed by the abundance of carbonaceous fragments, scours and pebbles, and locally stressed conditions. However, the presence of Slm, Spl and Shcs facies suggests shallow-wave reworking processes of these distal delta front deposits and the moderately intense bioturbation also suggests a transition between lower shoreface and distal delta front facies. On the other hand, the presence of coarse sandstones overlying scoured surfaces suggests bedload deposition by fluvial currents and considering the association with planar- and trough cross-stratified (subaqueous 2D/3D dunes) beds we interpreted them as terminal distributary channels (Olariu & Bhattacharya, 2006). The muddy partings might suggest the influence of minor tides or abandonment of the active channels. Dune-scale trough cross-bedding (FA6b) suggests high-energy currents able to develop 3D dunes migrating seaward, such a high-energy regime being supported by the paucity of bioturbation and frequent scour-and-fill structures, which in turn suggest the landward connection of these subaqueous dunes with terminal distributary channels (FA6c). The FA6b can be interpreted as short clinoform sets developed in a distal mouth bar, possibly indicating the rollover point of the delta front (Bhattacharya, 2010; Le Roux *et al*., 2010; Schwartz & Graham, 2015). In general terms, the association of terminal distributary channels (FA6c) and mouth bar complexes (FA6b) allow us to infer a delta front environment.

3.7 Facies association 7 (FA7): Fluvial deposits

This association only occurs in the northern sections SD, and CP (Table 1; Fig. 2) and is restricted to the upper part of the Dorotea Formation. It is characterized by 1 – 10 m thick, tabular to lenticular, finning-upward units. They overlie erosion surfaces mantled with pebble and/or shell lag; the tops are sharp or wavy. In the section SD these fining-upward successions show medium-grained sandstones that are high-angle planar cross-laminated or massive (Spa, Sm), followed by mottled, fine- to very fine-grained sandstone with ripple remnants (Sr), planar lamination (Spl), and plant remains or carbonized wood at the top. The section CP is more complex both laterally and vertically, comprising prominent lenticular to channeliform morphological ridges (Fig. 4i), enclosed in interbedded wavy laminated, very fine-grained sandstones and siltstones (Sw) with laminated or massive mudrocks (Fh, Fm) (poorly exposed by vegetation). The isolated bodies (Fig. 4i) range from 44 – 140 m long (along strike) and from 5 – 26 m thick. Internally, they are composed by erosionally based, poorly selected, matrix-supported, massive to normally graded conglomerate (Gmm, Gmg) (rarely showing bedding planes) with large sub-angular clasts (up to 1 m in diameter; Fig. 4m) of massive, greenish mudstone and shell hash, as well as carbonaceous fragments and sub-rounded andesitic pebbles dispersed throughout the unit. In addition, there are massive and trough cross-stratified, medium-grained sandstone packages (Sm, St), and fining-upward successions with rip-up clasts (or shell lag mantling a scoured surface; Fig. 4j) at the bases, rippled sandstones (Sr), laminated sandstones and siltstones (Spl, Slh) with abundant organic matter, carbonized trunks and pedogenic features in some layers (Fig. 4k, l).

This facies association clearly exhibits processes related to bedload deposition in a variable-energy, fluvial setting (Miall, 2014). The fining-upward succession with scoured bases, trough and tabular cross-laminated beds (Spa, St) followed by ripple-laminated sandstones (Sr) and laminated (commonly bioturbated) tops (Spl, Slh) represent point-bar deposits of meandering

rivers; although the presence of carbonaceous material, shell lags, and wavy tops on channels suggest occasional wave reworking (Fig. 4j). The overbank deposits (Fig. 4k) are represented by the muddy and silty units with wavy, and planar lamination (floodplain) and by the laminated and rippled beds (Spl, Slh, Sr) where organic matter, wood fragments, and pedogenetic nodules are present (crevasse splays). The coarse-grained, sediment-rich units represent bed-load deposits of braided rivers, where traction currents (St and Spl facies) and plastic (Gmm facies), and/or pseudoplastic (Gmg) debris flows were the two main depositional mechanisms.

3.8 Facies association 8 (FA8): Estuarine deposits

This facies association occurs exclusively in the upper Dorotea Formation (section SD; Table 1; Fig. 2, 4d) and comprises two sub-facies associations. The FA8a comprises a 70 m thick, fining-upward succession of sub-tabular geometry and complex lateral facies relationships, composed from the base up of massive, pebbly sandstone (Sm) with abundant shelly layers followed by massive, well-stratified, upper-medium-grained sandstones (Sm) grading to lower-medium-grained, tangential trough cross-bedded (~50 cm height) sandstones (St) with reactivation surfaces and capped by bidirectional-cross stratified beds (Shb) (Fig. 5f) showing mud lenses/partings often intercalated with horizontal-planar laminated sandstones (Spl). The succession continues with fine- to very fine-grained sandstone showing trough cross-stratification (St; ~1 m wavelength and < 0.15 m height; Fig. 5h) and upper plane lamination (Spl) shifting laterally to medium-grained, cross-bedded sandstones (Spa, St, Shb) (Fig. 5i,g) with scour-and-fill structures, mud drapes and tidal rhythmite (Hlh) intercalations. The FA8b consists of a 60 m thick, laterally continuous (km scale) succession comprised by interbedded mudstones/siltstones and very fine-grained sandstones (Hlh) with well-developed horizontal-planar lamination, in some cases with a low angle (seaward) inclination (Fig. 5j). These are commonly interrupted by scoured,

lenticular to sub-tabular, medium- to fine-grained, massive, coarsening-upward, shelly sandstones and conglomerates (Sm, Gs) (Fig. 5k) with upper plane laminated tops (Spl), or by fine- to very fine-grained sandstone beds with herringbone (Shb) (Fig. 5e), epsilon or tangential-based, trough cross-lamination with mud drapes (St). A 15 m thick, crudely fining-upward (medium- to fine-grained) tabular sandstone, divide the succession into two segments and is characterized by well-stratified, massive to low-angle planar cross-laminated sandstones (Sm, Spl) with diffuse cross-lamination (Sr) and numerous conglomeratic shelly lenses (Gs). More restricted is a 15 m thick succession of interbedded greenish, laminated, carbonaceous shales (Fh) with lignite streaks, and massive siltstones (Slm). Pervasive bioturbation dominates in the heterolithic facies of FA8b and some *Skolithos* isp. (Fig. 6l), can be observed in the top of the FA8a.

The FA8a represents the high-energy estuary mouth complex, where massive, pebbly sandstone associated with Spl facies and shelly layers can be interpreted as barrier spit and washover deposits; the presence of massive to low-angle planar laminated, fine-grained sandstones (Sm, Spl) suggests a foreshore setting (Le Roux *et al*., 2010). The overlying cross-bedded succession represents the tidal inlet channel and flood tidal delta, where some architectural elements can be observed. The medium-scale, tangential, trough cross-bedded sandstones (St) with abundant reactivation surfaces indicate the active (and deep) inlet channel whereas the bidirectional cross-bedded (Shb) and trough cross-laminated sandstone (St) with common clay lenses signal a shallow channel, which in turn grades into the spit platform represented by washed-out megaripples and upper-flow planar lamination in fine-grained sandstones (Reinson, 1992). The scoured bases mantled with pebble lag of the Spa facies, associated with Shb and St sandstones, are compatible with 2D/3D dunes of the shield and ebb spit, whereas Hlh facies could represent

the intertidal flat of the flood tidal delta (Boothroyd, 1985). The rare bioturbation and presence of S*kolithos* isp. reflect high-energy conditions of deposition.

In the FA8b, the large-scale, low-angle inclined heterolithic units (Hlh) are interpreted as sandy tidal mudflats (*sensu* Flemming, 2000) near the river mouth, with a slight depositional gradient towards the central basin. The horizontal-planar lamination on the tops of the sandstones and shelly conglomerates that are intercalated within the sandy tidal mudflats, and the planar-laminated fine-grained sandstones (Spl) could indicate wave action on local submerged sandy and/or shelly bars, or local beaches developed along the edge of the tidal flats, respectively (Le Roux *et al*., 2010). The fining-upward sandstones with Shb, and St facies and paired mud drapes are interpreted as point bar deposits of tidal creeks dominated by tidal processes, but the lateral relationship with the coarsening-upward, and inverse graded shelly sandstones and conglomerates (Fig. 5k) evidence shifting turbulent current signals of fluvial energy. The thick, tabular, fining-upward, sandstone bed dividing the succession is interpreted as distal distributary mouth bars affected by dense underflows and/or seasonal river discharges transporting brackish water fauna (Plink-Björklund, 2008; Le Roux *et al*., 2010). The Fh facies associated with coal streaks and siltstones (Slm), suggests deposition by suspension during low-energy conditions but frequently punctuated by clastic influx in a marsh plain surrounding the landward side of a lagoon or tidal flat. The overall FA8b represents a middle estuary sub-environment.

3.9 Facies association 9 (FA9): Prograding deep-water turbidite lobes

This facies association occurs exclusively in the Chorrillo Chico Formation (sections RB, PP, PC; Table 1; Fig. 2). In section RB, it consists of a coarsening- and thickening-upward succession. However, in the other sections a clear stacking pattern cannot be discerned. The FA9 is characterized by sharp-based, massive to normally graded, glauconitic siltstones (Slm) and very

fine- to medium-grained sandstones (Sm) that comprise individual units of 10 – 90 cm-thick, interbedded with thick mudstone beds (Fm) or massive siltstones (Slm). Ninety cm to 1.2 m thick, amalgamated beds comprised of (from the base upward) medium-grained, massive sandstones (Sm) with bases slightly erosive to planar, are followed by fine-grained, wispy, planar- or ripple-laminated sandstones (Sw, Spl, Sr) that grade to convolute layers (Fig. 5b) or siltstone/mudstone intercalations capped by mudstone beds (Fm). In section PP, the basal part of the formation shows mudstones (Fm) with alternating bioturbated (clean or glauconitic), fine-grained sandstones (Sm) with loading bases and flames (Fig. 5d). Angular flakes of coaly wood fragments (aligned preferentially NNW; Fig. 9b), angular to sub-angular glauconite and pumices pebbles can be recognized filling scours. Contorted bedding in mudstones and sandstones (Fig. 5b), and turboglyphs are common. Bioturbation is intense (BI is 3 – 6) and characterized by ichnogenera such as *Thalassinoides* isp., *Neonereites* isp. (Fig. 6b), *Scolicia* (*Laminites*) (Fig. 6c), *Asterosoma* isp., *Zoophycos* isp., *Phycosiphon incertum, Planolites* isp*., Chondrites* isp., *Ophiomorpha nodosa, Rhizocorallium* isp. (Fig. 6g), *Paradictyodora* ? *Taenidium barreti*, *Nereites missourensis* and local occurrences of *Skolithos* isp..

The individual beds are interpreted as a low-density turbiditic deposits, because the basal tool marks, tractional structures and normal grading indicates layer-by-layer deposition under turbulent and subsequent waning flow conditions (Covault *et al*., 2009; Haughton *et al*., 2009). Massive sandstone beds (Ta), wispy, planar- or ripple-laminated sandstones (Tb, Tc), as well as interbedded siltstones and mudstones (Td) capped by mudstones beds (Te) correspond to Bouma sequences (Fig. 5c). However, the presence of angular, coaly wood fragments (Fig. 9b), glauconite, and pumice pebbles within a fine-grained matrix filling scours is interpreted as debris-flow deposits (H3) and together with the alternating bioturbated (clean or glauconitic) sandstones (H2,

H1) within mudstones could represent internal sub-divisions of hybrid beds (Haughton *et al*., 2009) linked to the turbiditic deposits. The trace fossil assemblage shares characteristic of Zoophycos, and Nereites ichnofacies (Buatois & Mángano, 2011) and considering the benthic foraminifera content (Charrier & Lahsen, 1969; Rivera, 2017) suggests deep-water deposition close to a distal slope environment. Thus, the coarsening- and thickening-upward trend in section RB, reflects the existence of actively prograding turbidite lobes where the outer fan and fan-fringe are represented by sections PP, and PC.

4. DETRITAL ZIRCON GEOCHRONOLOGY AND SANDSTONE PETROGRAPHY

4.1 Method and dataset

Medium-grained sandstones samples were used preferentially for both petrography and zircon separation at the Geology Department of the University of Chile, following standard techniques. Samples RB1 and PB1 were collected from the lower part of the Chorrillo Chico Formation, whereas sample ZPR1 and ZLP1 corresponds to the lower and upper part of the Rocallosa Formation, respectively (Fig. 3a, b). The RB1 sample was dated by U-Pb using LA-MC-ICP-MS at the Mass Spectrometry Laboratory (CEGA) of the University of Chile, whereas the ZPR1, ZLP1 samples were dated by using LA-ICP-MS at the Laboratory of Isotopic Studies of the Geosciences Centre, Mexico (UNAM) and the PB1 sample at the Geochronology Laboratory of SERNAGEOMIN by using LA-ICP-MS. A detailed description of the geochronological method and raw data can be found in Appendix A and Table A1, respectively. Twenty-four fine- to medium-grained samples were selected to conduct 310 to 500 grain point counting by thin section using the Gazzi-Dickinson method and then normalized to quartz-feldespar-lithic (QFL), and monocrystalline quartz-feldespar-total lithic (Q_mFL_t) to be compared

on ternary plots with tectonic fields of Dickinson (1985) (Fig. 8). Point-counting raw data are represented in Table A2.

4.2 Maximum depositional ages from detrital zircons

To determine the maximum depositional age (MDA) from detrital zircons (DZ) in U-Pb geochronology, we employed the weighted mean age of the youngest peak (≥ 2 grains within a 2σ-level error overlap; after Dickinson & Gehrels, 2009; Schwartz *et al*., 2017) of the age spectrum. We report each age with its mean square of the weighted deviation (MSWD) and the range of acceptable MSWD based on the number of analyses contributing to each calculation (after Mahon, 1996). For the PB1 sample, the MDA of the 5 grains that yield concordant ages (Fig. 7a) and constitute the youngest age peak is 65.4±4.3 Ma, with a favourable MSWD=2.0 value based on the grains considered in the calculation. We consider this age as a robust one as it is (1) consistent with fossil ages (Charrier & Lahsen, 1969; Quattrocchio, 2009; Carrillo-Berumen, *et al*., 2013), (2) the analysis has a good precision (max. standard error= 2%), and (3) the scatter of ages is statistically consistent (Mahon, 1996), suggesting a higher likelihood of the grains coming from a single age population. However, it is worth mentioning that calculating MDA for the 3 concordant younger grains (and excepting the youngest single grain), a less robust but younger age (60.7±7 Ma; MSWD=2.1, see Appendix A) can be obtained, which leads us to hypothesize an SE-NW diachroneity as a result of north-westward progradation of the sedimentary system. The MDA of the RB1 sample, based on the youngest detrital zircon component (n=9 grains; Fig. 7b), is 65.2±0.46 Ma with a favourable MSWD=0.61 value. We also consider this age as a robust one according to the same arguments presented for sample PB1.

The MDA of the ZLP1 sample is 67.7±1.2 Ma (n=3; Fig. 7c), with a favourable MSD=0.71 which is considered as robust. For the ZPR1 sample, the MDA based on the youngest detrital peak

within the 2σ-level error overlap (n=2 grains; Fig. 7d), is 73.5±1.3 Ma with an MSWD=0.21. Although this age is robust and consistent with the palaeontological age (late Campanian-Maastrichtian; Charrier & Lahsen, 1969; Castelli *et al*., 1992) it may represent an overestimated (older) age since the youngest zircon is 67.7±2.4 Ma.

4.3 Detrital modal composition

The sandstones can generally be classified as lithic arkose (Rocallosa, Dorotea, and Chorrillo Chico Formations) to feldespathic litharenite (Cabo Naríz beds). The mean composition of the Rocallosa-Dorotea ($Q_{34}F_{44}L_{22}$, $Qm_{25}F_{44}Lt_{30}$) and Chorrillo Chico ($Q_{34}F_{44}L_{22}$, $Qm_{27}F_{44}Lt_{30}$) Formations plot within a *dissected arc* field (Fig. 8), although some differences can be highlighted when studying in detail their detrital composition. The framework grains in the Rocallosa-Dorotea Formations include the same proportions of monocrystalline and polycrystalline quartz, while the feldspar grains are in the same proportions between plagioclase and potassium feldspar (commonly altered). However, the latter is dominated by microcline and orthoclase with perthitic textures (Fig. 9c). The lithic fragments are mainly volcanic and metamorphic (Fig. 9d), the former characterized by felsitic and microlitic textures (Fig. 9j) and the latter by micaceous schists (Fig. 9f), and (meta-) volcanic (Fig. 9h), as well as pelitic fragments accompanied by tremolite-actinolite and chlorite minerals. In the Chorrillo Chico Formation, the monocrystalline quartz of volcanic and plutonic origin (Fig. 9k) is dominant. It increases up-section and plagioclase is the main feldspar. However, samples closer to the Rocallosa contact are potassium-feldspar-rich and impoverished in lithic fragments. The dominant lithic fragments are of volcanic (mainly of microlitic, and lathwork texture; Fig. 9g, i), and sedimentary origin and in a lesser extent metamorphic (metapelites). Some devitrified volcanic lithics can be observed (Fig. 9e). The sedimentary fragment content increases

up-section, as do the chert and vitric shards. The glauconite grains are fragmented and reworked unlike those of the Rocallosa Formation, which are mainly authigenic.

The mean composition ($Q_{19}F_{31}L_{50}$, $Qm_{31}F_{44}Lt_{54}$) of the Cabo Naríz sandstones (misinterpreted as the Cerro Toro Formation in Romans *et al*., 2010) plot within the *transitional arc* domain (Fig. 8), which has a clear predominance in volcanic lithic content with microlitic and felsitic textures (Fig. 9g), and a minor proportion of low-grade metamorphic fragments (Fig. 9f). The proportion of both potassium-feldspar and monocrystalline quartz slightly outweigh their counterparts in all the samples studied. However, the Cabo Naríz beds' lower member samples (Sánchez *et al*., 2010) are enriched in potassium-feldspar, monocrystalline quartz, as well as metamorphic and felsitic volcanic lithic fragments.

Some relative compositional trends can be observed in the Chorrillo Chico Formation which modal signature of the basal samples are more related to the Basement uplift domain and for the uppermost samples to the Recycled orogen domain (Fig. 8). For the Cabo Naríz beds, a clear compositional trend cannot be observed despite the richness in K-feldspar and monocrystalline quartz of the lower member's samples. This lack of a clear trend is also shared by our Rocallosa-Dorotea Formations samples. Notwithstanding, it is worthy to note that comparing the modal signature of the Dorotea Formation (samples of Romans *et al*., 2010 in the UEP) with our own Dorotea-Rocallosa samples (in a southernmost position) and the Chorrillo Chico Formation versus the Cabo Naríz samples, a spatial rather than a temporal trend in the modal composition is apparent (Fig. 8). The latter, point out important provenance shifts in short distances (~60-90 Km) along strike the basin.

4.4 Provenance record inferred by U-Pb ages and compositional data

DZ U-Pb ages from sample RB1 range from 64 to 655 Ma and are characterized by 3 significant age peaks at 67, 77, and 95 Ma and a small peak at 108 – 113 Ma. Additionally, a few older grains of Early Cretaceous (134 Ma; 1 grain), and Paleozoic-Neoproterozoic (528 – 655 Ma; 2 grains) are present, while the absence of Late Jurassic grains (Fig. 7e) is also noteworthy. The DZ age distribution of sample PB1 ranges from 54 to 131 Ma and contains a dominant age peak at 65 – 100 Ma (Fig. 7e). A minor subpopulation indiscriminate from the probability density curve but differentiated from the raw data, ranges from 53 – 60 Ma (Paleogene), and 110 – 131 Ma (Early Cretaceous). In this sample the absence of Late Jurassic and much older grains is apparent. However, Hervé *et al*. (2004) and Álvarez *et al*. (2006) have found a few Late Jurassic and Paleozoic-Neoproterozoic grains in samples collected very close to our PB1 sample. The Cabo Naríz samples (Sánchez *et al*., 2010) show a dominant age peak at 75 Ma and other significant peaks at 58, 88 – 94, and 107 Ma, some minor age peaks at 131 and 161 Ma, and a few Paleozoic-Mesoproterozoic grains also being present (Fig. 7e). The DZ age spectrum in ZPR1 sample ranges from 67.7 to 276.5 Ma and shows 3 significant age peaks at 68-81, 93-107, and between 142-160 Ma and a small peak at 277 Ma (Fig. 7e). The DZ age distribution of sample ZLP1 is like that of ZPR1, ranging from 67.1 to 2204 Ma, with main peaks at 69 – 73, 92 – 108, and 146 – 171 Ma, but older zircon peaks at 272 – 315, 615 – 640, and 1930 – 2200 Ma are better represented.

Based upon the dominance of Late Cretaceous and Paleocene (~56 – 100 Ma) detrital zircons both in the Dorotea-Rocallosa and Chorrillo Chico-Cabo Naríz samples, we interpret a continuous delivery of arc material from the Southern Patagonian Batholith (Hervé *et al*., 2007), which is consistent with the modal composition dominated by volcanic lithics, monocrystalline quartz, and K-feldspar with perthitic exsolution indicating the erosion of an intermediate to mafic volcanic shield and exposure of the arc roots (Fig. 8). Jurassic and Palaeozoic-Paleoproterozoic

zircons and felsic volcanic lithics (Fig. 9i, j) associated with micaceous schist fragments (Fig. 9f) in the Dorotea-Rocallosa and Chorrillo Chico-Cabo Naríz Formations suggest the incorporation of silicic volcanic (Tobífera Formation) and metamorphic (Eastern Andean Metamorphic complexes; Hervé *et al*., 2003) source terrane in the hinterland to the west (Fig. 1a), which is consistent with the heavy mineral suite identified by Charrier & Lahsen (1969). However, we cannot discard the probable contribution of Palaeozoic zircons from the Río Chico-Dungeness Arch (Fig. 1a) for the Dorotea strata, since having been previously demonstrated by Gutiérrez *et al*. (2017) further north of our study area. The relative contribution from the Rocas Verdes Basin volcanic rocks, and/or coeval intrusives (Pankhurst *et al*., 2000; Hervé *et al*., 2007; Calderón *et al*., 2007) together with reworked grains of the Eastern Andean Metamorphic Complex (Hervé *et al*., 2003) appears to have been more significant during sedimentation of the upper parts of Rocallosa-Dorotea Formations compared to the Chorrillo Chico Formation (Fig. 7e). The overall DZ Jurassic and Paleozoic-Mesoproterozoic grains of the Cabo Naríz samples (Sánchez *et al*., 2010) are relatively more abundant (ca. 8%) than in the Chorrillo Chico samples (ca. 4%), highlighting possible differences and shifts in sediment dispersal patterns along the basin axis, which are more evident comparing the Dorotea Formation (UEP; Romans *et al*., 2010; Schwartz *et al*., 2017; Gutiérrez *et al*., 2017; this study) with the Rocallosa Formation (MP). Both the Chorrillo Chico Formation and the Cabo Naríz beds exhibit volcanic components of the Tobífera Formation (Fig. 9e, g) and basement metamorphic in their basal parts (Fig. 9f), which decreases up-section in opposition to the increase of microlitic volcanic lithics (Fig. 9g) and vitric shards fragments. In summary, whereas continuous input of detritus from the Southern Patagonian Batholith throughout the latest Cretaceous to Paleocene is apparent, the relative contribution of the remnants of the Rocas Verdes Basin and of the Andean metamorphic complexes tend to decrease

significantly by the Paleocene when take place an intermediate to felsic volcanism elsewhere in the basin well (Macellari *et al*., 1989).

5. PALYNOLOGY

5.1 Method and dataset

Three fine-grained sandstone samples from the Rocallosa Formation (Fig. 3a) were processed for palynomorphs following standard palynological methods. All slides are housed at the Laboratory of Paleopalynology of the Departamento de Ciencias de la Tierra, Universidad de Concepción under codes 1525, 1526, and 1527.

5.2 Results

Many of the species identified (Table 3) lack stratigraphic significance since they have been identified in other basins within a wide temporal and stratigraphic range. However, the association of *Podocarpidites marwickii*, for the first time recorded in the Maastrichtian of the Argentinean Santa Cruz Province (Freile, 1972; Archangelsky & Romero, 1974), with the Paleocene (Danian?) *Nothofagidites dorotensis* (Fig. 10d), and *Tricolpites* sp. recorded for the first time in the Patagonian basins, Antarctica, and Australia (Povilauskas, 2017) suggests a Maastrichtian – basal Danian age for the upper part of Rocallosa Formation. This age is consistent with those reported for the equivalent Monte Chico and Cerro Dorotea Formations in Argentina (Fig. 1b), and the López de Bertodano Formation on Seymour Island (Antarctic Peninsula) where a similar palynoflora association is present (Askin 1990; Bowman *et al*., 2014; Povilasukas, 2017). Similarly, it is consistent with U-Pb ages reported for both the Rocallosa Formation (Hervé *et al*., 2004; this study) and the overlying Chorrillo Chico Formation reported in this study.

From the three samples analysed in the Rocallosa Formation (Fig. 2c, 3a), the palynomorph content (Table 3) displays a terrestrial predominance over dinocysts, which are commonly poorly preserved but can tentatively be identified as *Spiniferites* sp. This dominance suggests proximity to the area of continental supply. The association of epiphytic fungi spores (Fig. 10a, b), *Botryococcus braunii* (Fig. 10i), dinocysts, and Pteridophyta (Fig. 10f, g) suggests a marginal estuarine/deltaic brackish environment with considerable influence of freshwater. It also reflects a highly alkaline and generally oligotrophic environment surrounded by poorly drained areas, likely developing local peat swamps on the damp rainforest floors, where an understory of shade-tolerant ferns could flourish (Palma-Heldt, 1983; Borel, 2007; Bowman *et al*., 20014). The rainforest envisaged would be of Weddellian affinity, which was dominant from the Campanian to the Paleocene, and the association of *Podocarpidites, Nothofagidites*, and Pteridophytes suggests that these dense forests flourished in low coastal areas and humid environments. Normally, *Araucariacites* and *Podocarpidites* flourish in elevated areas, but they have proven to be adaptable and can be linked to relatively low areas related to coastal and/or marsh environments. Particularly, *Araucariacites australis* has been associated with coastal environments in the Springhill Formation (Quattrocchio *et al*., 2006). On the other hand, *Araucariacites* and *Podocarpidites* characterize the temperate-cold rainforest of the austral regions (Palma-Heldt, 1983), whereas the Cyatheaceae currently develop in pantropical regions and their abundance would indicate hot and humid paleoclimatic conditions as well (Povilauskas, 2017), although they are more sensitive to variations in humidity than to temperature (Palma-Heldt, 1983). The *Nothofagidites* is the most important genus that inhabits the sub-Antarctic forests of Patagonia and are associated with areas of high humidity (Palma-Heldt, 1983; Herngreen *et al*, 1996) and temperate climate (Quattrocchio & Volkheimer, 2000, Carrillo-Berumen *et al*., 2013). Particularly the *Nothofagidites brassii* type

(Fig. 10c) is related to temperate-warm climates (mesothermal) and lower areas. The palynofloristic association and its relative percentage of abundance allow us to interpret a temperate to temperate-cold climate, most likely with punctual climatic fluctuations to temperate-warm conditions but distinctly humid for the Maastrichtian-Danian interval.

6. DISCUSSION

6.1 Evolution of depositional systems

An upward-shoaling cycle is represented by the Fuentes-Rocallosa Formations (Fig. 3a) and by the Tres Pasos-Dorotea Formations (Fig. 3b) in the southern and northern part of the basin, respectively. The topmost Fuentes Formation is characterized by outer shelf-upper slope environments grading rapidly to an offshore transition setting (Fig 3a), where the sedimentation mechanism was related to turbidity currents probably triggered by storm events. These turbidite/tempestite events favoured the colonization of opportunistic organisms, a mechanism that has proved to be effective to provide higher oxygenation and nutrients to an otherwise poorly oxygenated setting (Rivera *et al*., 2018). The cycle continued with the establishment of shoreface environments of the Rocallosa Formation (Fig. 3a) where waves and storms were the main sediment transport mechanisms. Palaeocurrents and provenance data suggest sediment dispersal from the fold-thrust belt in the west (Fig. 12a). In the UEP the shift from slope deposits of the Tres Pasos Formation (Gutiérrez *et al*., 2017) to a deltaic system of the Dorotea Formation signals this first cycle. The lower and middle part of the Dorotea Formation represent a deltaic depositional system (Fig. 3b) in which the influence of waves was significant, hindering the clear distinction between shoreface and delta front and inhibiting the development of a large number of terminal distributary channels (Olariu & Bhattacharya, 2006; Bhattacharya, 2010). Palaeocurrent directions

indicate progradation towards the south (Fig. 3b), although the provenance data (Fig. 7e) suggest sediment input from the west, unlike the upper part of the Dorotea Formation where the incised valley systems show a sediment dispersal pattern derived from the west and northwest and probably from the north-northeast. We support our interpretation of incised valleys by the recognition criteria outlined by Zaitlin *et al*. (1994): (1) the bounding erosion surface has a regional character (Fig. 11a); (2) it is composed of multi-storey channels that record an abrupt basin-ward facies shift (Fig. 3b); (3) the estuarine infill onlaps the valley walls in a landward direction (Fig. 4d). The internal vertical evolution of the incised valley fill is reflected by the transition from braided fluvial channels to a meandering fluvial system followed by a protected estuary environment affected by tides (Fig. 3b), which implies a mixed energy scenario for the incised valley system. Member D of the Rocallosa Formation (*sensu* Charrier & Lahsen, 1969) could be the equivalent to the fluvial deposits at the base of the incised valleys system as reflects a change to a higher-energy conditions. The facies presented in the stratigraphic column of the La Pesca Bay (Fig.3a; modified from Elgueta S., in Álvarez *et al*., 2006), which represent to the Member D of the Rocallosa Formation, suggest the establishment of a Gilbert-type delta dominated by stacked debris flow in a landward (west) position; the presence of the angular to sub-angular pebbles and cobbles dispersed in scoured coarse-grained sandstones in our section PE (Fig. 3a, 9a) could then be interpreted as the distal reach of this deltaic system. The estuary environment in the UEP is equivalent to the deep-marine facies of the Chorrillo Chico Formation and Cabo Nariz beds, representing jointly the change to a deepening cycle of environments within the basin. The coarsening- and thickening-upward trend in the Chorrillo Chico Formations and Cabo Nariz beds (Sánchez *et al.*, 2010) depicts a northwest-ward prograding turbidite fan system with continuous input from the arc and hinterland volcaniclastic and metamorphic source terranes in the south and

southwest (Fig. 12b). The inner channelized fan areas are in Tierra del Fuego, whereas the middle and distal outer fan-basin plain deposits are located in sections RB and PP (Table 1; Fig. 2c), respectively. Cohesive flows were an important process in the middle and distal fan system, most likely triggered by erosion of the shoreface as suggested by the highly fragmented and reworked glauconite grains, and by river flood discharge events (hyperpycnal flows) as the presence of terrestrially derived carbonized trunks indicates (Fig. 9b).

6.2 Sequence stratigraphic architecture

Our objective with the sequential stratigraphic framework is to provide a better understanding of the interplay of the depositional elements in time and space on a regional scale. Thus, at this scale, two (partial) sequences can be identified (Fig. 11a), which are equivalent to sequences 2 and 3 of Macellari *et al*. (1989). Tracing surfaces of sequential stratigraphic significance between the different stratigraphic sections and the recognition of a stratal stacking pattern is physically limited, therefore, our correlation and identification are based on changes of accommodation-sedimentation dynamics and vertical relationships between the sedimentary environments.

Sequence 1. The basal sequence boundary is well represented in the northernmost part of the basin (Lago Argentino) by the Campanian-Maastrichtian angular unconformity that separates the La Anita and La Irene Formations (Macellari *et al*., 1989). In our study area, this unconformity became a correlative conformity, although Mpodozis (in Álvarez *et al*., 2006) notes an unconformity between the Tres Pasos and Monte Chico-Dorotea Formations in the Cerro Cazador area. Given the paleo-bathymetric conditions of our study area, only the highstand system tract (HST) can be recognized (Fig. 11a). The latter is manifested (in UEP) by transition from shelf deposits of the Tres Pasos Formation (Gutiérrez *et al*., 2017) to deltaic deposits of the Dorotea

Formation (Fig. 11b). Internally, in the Dorotea Formation high-frequency parasequences (clinothems) with an aggrading to prograding stacking pattern (Fig. 11b) can be observed, denoting landward changes in the shoreline trajectory. In the MP, the HST is represented by the prograding shoreface deposits of the Rocallosa Formation underlying the aggrading outer shelf to upper slope environments (Fig. 11c) of the uppermost Fuentes Formation. This transition, in turn, marks the maximum flooding surface (MFS). The development of the HST mirrors a normal regression (Fig. 11c) where sedimentation tends to balance or outpace the rates of base-level rise, correspondingly with erosion in the fold-thrust belt and a progressive sea-level fall (Haq, 2014).

Sequence 2. The sequence boundary (~67 Ma) is an angular unconformity limiting the Calafate and Chorrillo Formations (in Lago Argentino; Macellari *et al*., 1989) correlatable with the regional incision surface at the base of the incised valleys in the UEP (Fig. 11a), which in turn becomes a correlative conformity in MP (Fig. 11a, b). The tectonic nature of this sequence boundary is reinforced by the presence of a depositional hiatus toward the forebulge (Mpodozis *et al*., 2011) interpreted as the result of tectonic loading. Immediately before the forced regression, the incised valleys were composed of a low-sinuosity fluvial system which is interpreted to reflect low-accommodation lowstand fluvial deposits (Fig. 3b), whereas in the MP the lowstand system tract (LST) is represented by the Gilbert-type delta in Member D of the Rocallosa Formation (Fig. 3a). In turn, the vertical change into a high-sinuosity fluvial style with well-developed floodplains in section CP, as well as a progressive marine influence on the low-amalgamated, fluvial channels in section SD, abruptly overlain by lagoon and mire deposits, indicate an increase in accommodation space (Fig. 11b). This larger accommodation space is reflected by the mudstone-dominated interval of the turbidite succession at the base of Chorrillo Chico Formation (Fig. 11c). The long-term evolution from a fully fluvial system in the north of the basin and upper shoreface

deposits in the south, that grade upward to a wave-dominated estuary and deep marine deposits, in the north and south of the basin, respectively, suggests a backstepping stacking pattern representing a transgressive system tract (TST) (Fig. 11b, c). The commencement of the TST is then interpreted by the well development of floodplains deposits (section CP) whereas the transgressive surface (TS) is interpreted by the wave-ravinement scouring (Fig. 4j) on the fluvial channels (in section SD and CP) in the UEP. The location of such a surface in the MP is more tedious, but it is assumed to be represented by the boundary between the Rocallosa and Chorrillo Chico Formations (Fig. 11c). We infer that the beginning of the bay-head delta development in the estuarine depositional system (Fig. 3b), implies the turnaround from transgression to regression. Therefore, we place an MFS at the base of the distal distributary mouth bars (in section SD; Fig. 11b) and in the transition to a sandstone-dominated turbidite system of the Chorrillo Chico Formation (Fig. 11c) that indicates the commencement of an HST, which in turn signals the larger sediment influx into the basin in an attempt to outpace the base-level rise. The uppermost sequence boundary is represented by ~15 Myr unconformity between the Dorotea (Maastrichtian-Danian) and Rio Turbio (Eocene) Formations in the UEP (e.g., Malumián & Caramés, 1997; Fosdick *et al*., 2011, 2015; Gutiérrez *et al*., 2017) whereas in the south (in the MP) is represented by the ~3 Myr gap between the Chorrillo Chico and Agua Fresca Formations (Rivera, 2017) reflected as a correlative conformity. It is important to mention the diachroneity of this sequence boundary, which initiates at ~61 Ma in the UEP and by ~58 Ma in the MP.

The importance of the accommodation space in terms of the development of either unconformities or correlative conformities and the constantly larger depth of the basin in the south is noteworthy, allowing the development of thicker parasequences. The latter illustrates the primary role and even long-term affectation of the inherited crustal configuration e.g., the

extensional phase of the Rocas Verdes Basin (Romans *et al*., 2010; Fosdick *et al*., 2011; McAtmaney *et al*., 2011) in the filling evolution, and response to tectonic events of a foreland basin system.

6.3 Role of climate

Most of the reported Patagonian transgressions are based on climatic optima (Malumián & Náñez, 2011). If we accept this hypothesis, one would expect an abundance of large foraminifera or thermophilic biota in a warm sea flooding Patagonia. However, these are absent, as also indicated by the latter authors. In contrast, oceanic conditions were predominantly cold since at least the late Santonian and lasted until the Danian (Barrera & Savin, 1999; Sial *et al*., 2001; Le Roux, 2012; Huber, 2018), which makes it imperative to evaluate the role of climate in a different way.

In the light of our palynological results (Table 3), we interpret a palaeoclimatic context of mainly temperate to cool temperate (~7-10.1°C), humid and rainy during the K-Pg interval, which may have prevailed since at least the early Maastrichtian (~70 Ma) according to recently reported megaflora results in the Dorotea Formation in the Sierra Baguales area (Pino *et al*., 2018), and from quantitative palynological results on Seymour Island (Marambio) in the Antarctic Peninsula (Bowman *et al*., 2014). In addition, a cool palaeoclimate during the K-Pg transition has also been suggested from independent evidence for both the Magallanes-Austral Basin and surrounding areas. Sial *et al*. (2001) interpreted a significant decrease in temperature at the K-Pg transition based on stable oxygen isotope records in the PR section (Table 1; Fig. 2b), stratigraphically correlating with the base of the Chorrillo Chico Formation. This cooling trend has also been documented elsewhere in the region, such as in the South Atlantic Ocean and the Antarctic Peninsula (Barrera & Savin, 1999; Huber, 2018).

This generalized cooling trend supports the sea-level fall recorded from the late Campanian (Haq, 2014) and together with the tectonic influence explains the occurrence of regressive stages in the basin, as detailed in the previous section. Therefore, the presence of palynomorphs indicative of warmer conditions (~15.2°C) in the Rocallosa Formation fits within the "warmth-loving" plant associations occupying coastal lower areas left by the regression, reflecting a vegetational zoning according to the altitudinal gradient in the nearby area into the accumulation zone (Askin, 1990).

6.4 Tectonic versus eustatic trigger of the Atlantic transgression

Previous research dealing with sea-level changes or the Maastrichtian-Danian transgression in Patagonia, unquestionably invoke eustatic forcing as the causative mechanism of base-level changes (Malumián & Nañez, 2011; Leppe et al., 2012; Vallekoop et al., 2017). However, the progressive decrease of the long-term eustatic sea-level from the late Campanian (Haq, 2014) challenges the eustatic factor as a plausible mechanism for the Atlantic transgression in Patagonia.

Certainly, local or regional tectonism is a reasonable alternative explanation for the origin of the transgression and only a few studies incorporate this mechanism (e.g., Aguirre-Urreta *et al*., 2011; Gianni *et al*., 2018) based on the coincidence of compressional phases with the transgressive event. To prove the controlling nature of regional tectonism on the transgression, a concomitant orogenic loading and flexural subsidence must be demonstrated. A tectonic event can be recognized by the existence of a regional basal incision surface resulting in incised valley systems (Fig. 3b, 11), as we demonstrated in previous sections; and a subsidence can be proved by examining the geometry of the basin-fill deposits during the time of the transgression and analyzing their burial history. Mpodozis *et al*. (2011) highlight the wedge geometry of the Maastrichtian-Paleocene deposits, which thicken westwards, preserving the asymmetric geometry

of a subsiding foreland basin. Furthermore, the burial history during deposition of the Dorotea Formation in UE reveals that it reached the maximum burial depth by the early Paleocene (Fig. 7 of Schwartz *et al*., 2017). Therefore, we postulate that the Patagonian orogenic load caused flexural subsidence able to sustain the first Atlantic-derived transgression in the Magallanes-Austral Basin.

6.5 Constraints on the timing of fold-thrust belt deformation

The sedimentary response of the Magallanes-Austral Basin has been critical to unravel the timing and style of deformation of the Patagonian orogenic wedge (Fildani *et al*., 2008; Romans *et al*., 2010; McAtamney *et al*., 2011; Gutiérrez *et al*., 2017) and complements structural geology studies that otherwise provide poor temporal constraints (Fosdick *et al*., 2011; Betka *et al*., 2015). The integration of our dataset allows us to highlight some phases of tectonic activity in the Magallanes-Austral Basin. However, it is important, bearing in mind that the evolution and sequence of unroofing of the fold-thrust belt vary along-strike in the basin because of the inherited basin configuration and the closure diachroneity of the Rocas Verdes Basin (Romans *et al*., 2010; Fosdick *et al*., 2011; McAtmaney *et al*., 2011).

During the first phase at ~85 – 82 Ma (sedimentation time of older Dorotea Formation deposits, cf. Romans *et al*., 2010; Schwartz *et al*., 2017), the metamorphic basement was already exposed (Romans *et al*., 2010; Gutiérrez *et al*., 2017) and the erosion of the volcanic arc was still incipient (*transitional arc* domain of Romans *et al*., 2010). By ~72 Ma the continuous exhumation of the hinterland gave rise to accentuated erosion of the arc (*dissected arc* domain; Fig. 8) and of the Andean metamorphic and Upper Jurassic silicic volcanic terranes (Tobífera Formation), which are reflected in the DZ (Fig. 7e) and modal signature of the younger deposits of the Dorotea-Rocallosa Formations (Fig. 9). The increases in sedimentation rates and shoaling of environments in the transition of the Tres Pasos-Fuentes to Dorotea-Rocallosa Formations within a normal

regressive context, can be ascribed to the latter processes. This protracted exhumation of the hinterland is consistent with crustal basement shortening and internal deformation in an orogenic growth phase and corresponds to an orogen-wide basement-involved faulting event (Fig. 12 a) (e.g., Fosdick *et al*., 2011; Betka *et al*., 2015).

A second phase characterized by a major thrusting event by the end of the Maastrichtian (~67 Ma) triggered a forced regression and the development of incised valleys (Fig. 11a) in the upper part of the Dorotea Formation (UEP). This caused an abrupt and dynamic depositional shift from a lower shoreface to a high-energy Gilbert-type delta (MP) (Fig. 11c) where a lesser accommodation space was available. This event uplifted the Andean metamorphic basement and Upper Jurassic-Lower Cretaceous rocks of the Rocas Verdes Basin, as is demonstrated by the modal composition of the upper Dorotea-Rocallosa, lower Cabo Naríz beds (and conglomerates clasts studied by Sánchez, 2006) and Chorrillo Chico Formation (Fig. 9). The latter is supported by Sr isotopic studies (Sial *et al*., 2001) that record changes in the dynamics of the orogen, inferring an early rise and subsequent erosion of the mountain range nearly to the K-Pg boundary. The tectonic loading caused a large accommodation space suitable for the establishment of estuarine deposits (UEP) and deep-marine turbidite sequences (MP and Tierra del Fuego). The transition from a thick- to thin-skinned structural style (Fig. 12b) is inferred by the incorporation of foredeep deposits in the most external fold-thrust belt, showing an up-section decrease in basement input and likewise an increase in the chert and sedimentary lithic content, which explain the orogen recycled trend in the Chorrillo Chico Formation by the end of Paleocene (~58 Ma).

7. CONCLUSIONS

The shift from outer shelf (Fuentes Formation) to a shoreface environment (Rocallosa Formation) reveal a highstand normal regression. The increasingly negative accommodation reached its climax during the development of incised valleys (upper Dorotea Formation) and Gilbert-type delta (member D of the Rocallosa Formation) within a forced regression context. This generalized regression may have been the right time to enable a biogeographic land bridge between Patagonia and the Antarctic Peninsula, allowing the observed palaeofaunistic and palaeofloristic exchange (Leppe *et al*., 2012).

We postulate that the origin of Maastrichtian-Danian transgression is linked to tectonic forcing during a generalized cool climate and that the stratigraphic record is marked by the estuarine deposits and deep-water turbidites in the uppermost Dorotea and Chorrillo Chico Formations, respectively, as a response to the positive accommodation space available.

The K-Pg boundary can be delineated in better detail at the contact between the Monte Chico and Cerro Dorotea Formations (Rio Turbio, Argentina) corresponding to the upper part of the Chilean Dorotea Formation and closer to the base of Chorrillo Chico Formation.

Our results strengthen the idea that the Southern Patagonian Batholith maintained its proximity and connectivity with the foredeep, a feature that differentiates the Magallanes Basin from Andean-type foreland basins elsewhere. It also provides evidence of the influx of sediments sourced in the Andean metamorphic complexes, and the Rocas Verdes Basin terrane as result of an unroofing episode which feeds Maastrichtian-Danian strata.

We conclude that a major thrusting event took place at ~67.7 Ma, resulting in the development of a regional discordance traceable throughout the basin and surrounding areas, but in areas of larger accommodation space this unconformity became a correlative conformity as is the case in the Magallanes Province. Additionally, we hypothesize that the disappearance of the

Maastrichtian endemic foraminifera species (Malumián & Náñez, 2011) is linked to this regional event.

ACKNOWLEDGEMENTS

This study was financially and logistically supported by FONDECYT projects 1130006 and 1161806, and by the CONICYT-PFCHA-National Doctoral Scholarship 2017 No. 21170419. L.K. Sánchez and I.A. Gómez (Universidad de Chile) are thanked for their invaluable assistance during field campaigns and A.V. Poblete for support in palynological analysis. We gratefully acknowledge L. Rojas (Enap-Sipetrol) for permission to review unpublished reports and collaboration in this research. We thank L. Buatois for his very kind and helpful assistance in the identification of some ichnological traces, M. Leisen (CEGA), L. Solari (UNAM), M. Suárez and F. Llona (SERNAGEOMIN) are thanked for detrital zircon age dating and analysis. We thank J. Martinod (USMB) for discussion about Patagonian Andes tectonics and comments on an early version of the manuscript.

CONFLICTS OF INTEREST

No conflict of interest to declare.

REFERENCES

Aguirre-Urreta, B., Tunik, M., Naipauer, M., Pazos, P., Ottone, E., Fanning, M., & Ramos, V. A. (2011). Malargüe Group (Maastrichtian–Danian) deposits in the Neuquén Andes, Argentina: Implications for the onset of the first Atlantic transgression related to Western

Gondwana break-up. *Gondwana Research*, *19*(2), 482-494. https://doi.org/10.1016/j.gr.2010.06.008

Álvarez, P., Elgueta, S., Mpodozis, C., Briceño, M., Vieytes, H., Radic, J. P., Mella, P. (2006). Revisión de la estratigrafía y facies de la cuenca de antepaís Cretácica entre Lago Argentino y Península Brunswick. Proyecto Tranquilo-Otway, Informe Final. Empresa Nacional de Petróleo (ENAP), Unpublished technical report, 290 p.

Archangelsky, S., & Romero, E. J. (1974). Polen de gimnospermas (coníferas) del Cretácico Superior y Paleoceno de Patagonia. *Ameghiniana*, *11*(3), 217-236.

Askin, R. A. (1990). Campanian to Paleocene spore and pollen assemblages of Seymour Island, Antarctica. *Review of Palaeobotany and Palynology*, *65*(1-4), 105-113.

Barrera, E., & Savin, S. M. (1999). Evolution of late Campanian-Maastrichtian marine climates and oceans. *Special Papers-Geological Society of America*, 245-282.

Betka, P., Klepeis, K., & Mosher, S. (2015). Along-strike variation in crustal shortening and kinematic evolution of the base of a retroarc fold-and-thrust belt: Magallanes, Chile 53° S–54°. *Geological Society of America Bulletin*, *127*(7-8), 1108-1134. https://doi.org/10.1130/B31130.1

Bhattacharya, J. P. (2010) Deltas. In N. P., James & R. W., Dalrymple (Eds.), Facies Models 4 (pp. 233-264). St. John's, Newfouland & Labrador: Geological Association of Canada.

Boothroyd, J. C. (1985). Tidal inlets and tidal deltas. In *Coastal sedimentary environments* (pp. 445-532). Springer, New York, NY.

Borel, C. M. (2007). Algas no silíceas y acritarcos de depósitos costeros holocenos en el arroyo La Ballenera, Buenos Aires, Argentina. *Ameghiniana*, *44*(2), 359-366.

Bowman, V. C., Francis, J. E., Askin, R. A., Riding, J. B., & Swindles, G. T. (2014). Latest Cretaceous–earliest Paleogene vegetation and climate change at the high southern latitudes: palynological evidence from Seymour Island, Antarctic Peninsula. *Palaeogeography, Palaeoclimatology, Palaeoecology*, *408*, 26-47. https://doi.org/10.1016/j.palaeo.2014.04.018

Buatois, L. A., & Mángano, M. G. (2011). *Ichnology: Organism-substrate interactions in space and time*. Cambridge University Press.

Calderón, M., Fildani, A., Herve, F., Fanning, C. M., Weislogel, A., & Cordani, U. (2007). Late Jurassic bimodal magmatism in the northern sea-floor remnant of the Rocas Verdes basin, southern Patagonian Andes. *Journal of the Geological Society*, *164*(5), 1011-1022.

Carrillo-Berumen, R., Quattrocchio, M. E., & Helenes, J. (2013). Paleogene continental Palynomorphs of the formations Chorrillo Chico and Agua Fresca, Punta Prat, Magallanes, Chile. *Andean Geology*, *40*(3), 539-560. http://dx.doi.org/10.5027/andgeoV40n3-a08

Castelli, J. C., Robertson, R., Harambour, S. (1992). Evaluación Geológica y Petrolera, bloques Última Esperanza Sur e Isla Riesco. Empresa Nacional de Petróleo (ENAP), Unpublished technical report, 160 p.

Catuneanu, O. (2004). Retroarc foreland systems—evolution through time. *Journal of African Earth Sciences*, *38*(3), 225-242. https://doi.org/10.1016/j.jafrearsci.2004.01.004

Charrier, R., & Lahsen, A. (1969). Stratigraphy of Late Cretaceous-Early Eocene, Seno Skyring--Strait of Magellan Area, Magallanes Province, Chile. *American Association of Petroleum Geologist Bulletin*, *53*(3), 568-590.

Covault, J. A., Romans, B. W., & Graham, S. A. (2009). Outcrop expression of a continental-margin-scale shelf-edge delta from the Cretaceous Magallanes Basin, Chile. *Journal of Sedimentary Research*, *79*(7), 523-539. https://doi.org/10.2110/jsr.2009.053

Dalziel, I. W. D. (1981). Back-arc extension in the southern Andes: a review and critical reappraisal. *Philosophical Transactions of the Royal Society of London. Series A, Mathematical and Physical Sciences*, *300*(1454), 319-335.

Dickinson, W. R. (1985). Interpreting provenance relations from detrital modes of sandstones. In *Provenance of arenites* (pp. 333-361). Springer, Dordrecht.

Dickinson, W. R., & Gehrels, G. E. (2009). Use of U–Pb ages of detrital zircons to infer maximum depositional ages of strata: a test against a Colorado Plateau Mesozoic database. *Earth and Planetary Science Letters*, *288*(1-2), 115-125. https://doi.org/10.1016/j.epsl.2009.09.013

Dott Jr, R. H., & Bourgeois, J. (1982). Hummocky stratification: significance of its variable bedding sequences. *Geological Society of America Bulletin*, *93*(8), 663-680.

Dumas, S., & Arnott, R. W. C. (2006). Origin of hummocky and swaley cross-stratification—The controlling influence of unidirectional current strength and aggradation rate. *Geology*, *34*(12), 1073-1076. https://doi.org/10.1130/G22930A.1

Fildani, A., Romans, B. W., Fosdick, J. C., Crane, W. H., & Hubbard, S. M. (2008). Orogenesis of the Patagonian Andes as reflected by basin evolution in southernmost South America. *Arizona Geological Society Digest*, *22*, 259-268.

Flemming, B. W. (2000). A revised textural classification of gravel-free muddy sediments on the basis of ternary diagrams. *Continental shelf research*, *20*(10-11), 1125-1137. https://doi.org/10.1016/S0278-4343(00)00015-7

Fosdick, J. C., Romans, B. W., Fildani, A., Bernhardt, A., Calderón, M., & Graham, S. A. (2011). Kinematic evolution of the Patagonian retroarc fold-and-thrust belt and Magallanes foreland basin, Chile and Argentina, 51 30′ S. *Geological Society of America Bulletin*, *123*(9-10), 1679-1698. https://doi.org/10.1130/B30242.1

Fosdick, J. C., Grove, M., Graham, S. A., Hourigan, J. K., Lovera, O., & Romans, B. W. (2015). Detrital thermochronologic record of burial heating and sediment recycling in the Magallanes foreland basin, Patagonian Andes. *Basin Research*, *27*(4), 546-572. https://doi.org/10.1111/bre.12088

Freile, C. (1972). Estudio palinologico de la formacion cerro dorotea (Maestrichtiano-Paleoceno) de la provincia de Santa Cruz. I. *Revista del Museo de La Plata*, *6*(38), 39-63.

Gianni, G. M., Echaurren, A., Fennell, L., Navarrete, C. R., Quezada, P., Tobal, J., ... & Folguera, A. (2018). Cretaceous Orogeny and Marine Transgression in the Southern Central and Northern Patagonian Andes: Aftermath of a Large-Scale Flat-Subduction Event? In *The Evolution of the Chilean-Argentinean Andes* (pp. 291-328). Springer, Cham. https://doi.org/10.1007/978-3-319-67774-3_12

Gutiérrez, N. M., Le Roux, J. P., Vásquez, A., Carreño, C., Pedroza, V., Araos, J., ... & Hinojosa, L. F. (2017). Tectonic events reflected by palaeocurrents, zircon geochronology, and palaeobotany in the Sierra Baguales of Chilean Patagonia. *Tectonophysics*, *695*, 76-99. https://doi.org/10.1016/j.tecto.2016.12.014

Haq, B. U. (2014). Cretaceous eustasy revisited. *Global and Planetary change*, *113*, 44-58. https://doi.org/10.1016/j.gloplacha.2013.12.007

Haughton, P., Davis, C., McCaffrey, W., & Barker, S. (2009). Hybrid sediment gravity flow deposits–classification, origin and significance. *Marine and Petroleum Geology*, *26*(10), 1900-1918. https://doi.org/10.1016/j.marpetgeo.2009.02.012

Herngreen, G. F. W., Kedves, M., Rovnina, L. V., & Smirnova, S. B. (1996). Cretaceous palynofloral provinces: a review. In J., Jansonius, & D.C., McGregor, (Eds.), Palynology: Principles and Applications (pp. 1157-1188). American Association of Stratigraphic Palynologists Foundation.

Herve, F., Fanning, C. M., & Pankhurst, R. J. (2003). Detrital zircon age patterns and provenance of the metamorphic complexes of southern Chile. *Journal of South American Earth Sciences*, *16*(1), 107-123. https://doi.org/10.1016/S0895-9811(03)00022-1

Hervé, F., Godoy, E., Mpodozis, C., Fanning, M. (2004). Monitoring magmatism of the Patagonian Batholith trough the U-Pb SHRIMP dating of detrital zircons in sedimentary units of the Magallanes basin. International Symposium on the Geology and Geophysics of the Southernmost Andes, the Scotia Arc and Antartic Peninsula (GEOSUR). *Bollettino di Geofisica teorica ed applicata*, *45*(Suppl. 2), 1-281.

Herve, F., Pankhurst, R. J., Fanning, C. M., Calderón, M., & Yaxley, G. M. (2007). The South Patagonian batholith: 150 my of granite magmatism on a plate margin. *Lithos*, *97*(3-4), 373-394. https://doi.org/10.1016/j.lithos.2007.01.007

Huber, B. T., MacLeod, K. G., Watkins, D. K., & Coffin, M. F. (2018). The rise and fall of the Cretaceous Hot Greenhouse climate. *Global and planetary change*, *167*, 1-23. https://doi.org/10.1016/j.gloplacha.2018.04.004

Leppe, M., Mihoc, M., Varela, N., Stinnesbeck, W., Mansilla, H., Bierma, H., ... & Jujihara, T. (2012). Evolution of the Austral-Antarctic flora during the Cretaceous: New insights from a paleobiogeographic perspective. *Revista Chilena de Historia Natural, 85,* 369-392.

Le Roux, J. P., Nielsen, S. N., & Henríquez, Á. (2008). Depositional environment of Stelloglyphus llicoensis isp. nov.: a new radial trace fossil from the Neogene Ranquil Formation, south-central Chile. *Andean Geology*, *35*(2), 307-320. http://dx.doi.org/10.4067/S0716-02082008000200006

Le Roux, J. P., Puratich, J., Mourgues, F. A., Oyarzún, J. L., Otero, R. A., Torres, T., & Hervé, F. (2010). Estuary deposits in the Río Baguales Formation (Chattian-Aquitanean), Magallanes Province, Chile. *Andean Geology*, *37*(2), 329-344.

Le Roux, J. P. (2012). A review of Tertiary climate changes in southern South America and the Antarctic Peninsula. Part 1: Oceanic conditions. *Sedimentary Geology*, *247*, 1-20. https://doi.org/10.1016/j.sedgeo.2011.12.014

Macellari, C. E., Barrio, C. A., & Manassero, M. J. (1989). Upper Cretaceous to Paleocene depositional sequences and sandstone petrography of southwestern Patagonia (Argentina and Chile). *Journal of South American Earth Sciences*, *2*(3), 223-239.

Mahon, K. I. (1996). The New "York" regression: Application of an improved statistical method to geochemistry. *International Geology Review*, *38*(4), 293-303. https://doi.org/10.1080/00206819709465336

Malumián, N., & Caramés, A. (1997). Upper Campanian-Paleogene from the Río Turbio coal measures in southern Argentina: micropaleontology and the Paleocene/Eocene boundary. *Journal of South American Earth Sciences*, *10*(2), 189-201. https://doi.org/10.1016/S0895-9811(97)00015-1

Malumian, N., & Nanez, C. (2011). The Late Cretaceous–Cenozoic transgressions in Patagonia and the Fuegian Andes: foraminifera, palaeoecology, and palaeogeography. *Biological Journal of the Linnean Society*, *103*, 269-288. https://doi.org/10.1111/j.1095-8312.2011.01649.x

McAtamney, J., Klepeis, K., Mehrtens, C., Thomson, S., Betka, P., Rojas, L., & Snyder, S. (2011). Along-strike variability of back-arc basin collapse and the initiation of sedimentation in the Magallanes foreland basin, southernmost Andes (53–54.5° S). *Tectonics*, *30*(5). https://doi.org/10.1029/2010TC002826

MacDonald, D. I. (1986). Storm-generated sandstone beds from the Upper Cretaceous of south Chile and their regional significance. *Andean Geology*, (28-29), 69-76. http://dx.doi.org/10.5027/andgeoV13n2-3-a04

MacEachern, J. A., Bann, K. L., Bhattacharya, J. P., & Howell Jr, C. D. (2005). Ichnology of deltas: organism responses to the dynamic interplay of rivers, waves, storms, and tides. In L., Giosan & J. P., Bhattacharya (Eds.), River deltas: concepts, models and examples (pp. 65-93). SEPM Special Publications vol. 83.

Miall, A. D. (2014). *Fluvial depositional systems* (Vol. 14). Berlin: Springer.

Mitrovica, J. X., Beaumont, C., and Jarvis, G. T. (1989). Tilting of continental interiors by the dynamical effects of subduction. *Tectonics, 8,* 1079–1094. https://doi.org/10.1029/TC008i005p01079

Mpodozis, C., Mella, P., & Padva, D. (2011). Estratigrafía y megasecuencias sedimentarias en la cuenca Austral-Magallanes, Argentina y Chile. VII Congreso de Exploración y Desarrollo de Hidrocarburos, Simposio Cuencas Argentinas: visión actual, pp. 97-137.

Myrow, P. M., Fischer, W., & Goodge, J. W. (2002). Wave-modified turbidites: combined-flow shoreline and shelf deposits, Cambrian, Antarctica. *Journal of Sedimentary research*, *72*(5), 641-656. https://doi.org/10.1306/022102720641

Náñez, C., & Malumián, N. (2008). Paleobiogeografía y paleogeografía del Maastrichtiense marino de la Patagonia, Tierra del Fuego y la Plataforma Continental Argentina, según sus foraminíferos bentónicos. *Revista Española de Paleontología*, *23*(2), 273-300.

Olariu, C., & Bhattacharya, J. P. (2006). Terminal distributary channels and delta front architecture of river-dominated delta systems. *Journal of sedimentary research*, *76*(2), 212-233. https://doi.org/10.2110/jsr.2006.026

Quattrocchio, M. E., & Volkheimer, W. (2000). Paleoclimatic changes during the Paleocene-Lower Eocene in the Salta Group Basin, NW Argentina. In *Southern Hemisphere Paleo- and Neoclimates* (pp. 353-367). Springer, Berlin, Heidelberg.

Quattrocchio, M. E., Martínez, M. A., Pavisich, A. C., & Volkheimer, W. (2006). Early Cretaceous palynostratigraphy, palynofacies and palaeoenvironments of well sections in northeastern Tierra del Fuego, Argentina. *Cretaceous Research*, *27*(4), 584-602. https://doi.org/10.1016/j.cretres.2005.11.012

Quattrocchio, M. E. (2009). Paleogene dinoflagellate cysts from Punta Prat, southern Chile. *Palynology*, *33*(1), 141-156. https://doi.org/10.2113/gspalynol.33.1.141

Palma-Heldt, S. (1983). Estudio palinológico del Terciario sedimentario de Lonquimay, provincia de Malleco, Chile. *Andean Geology*, (18), 55-75.

Pankhurst, R. J., Riley, T. R., Fanning, C. M., & Kelley, S. P. (2000). Episodic silicic volcanism in Patagonia and the Antarctic Peninsula: chronology of magmatism associated with the

break-up of Gondwana. *Journal of Petrology*, *41*(5), 605-625. https://doi.org/10.1093/petrology/41.5.605

Pino, J. P., Leppe, M., Trevisan, C., Wilberger, T., Manríquez, L., Fernández, R., … Lobos, V. (2019). Los ensambles vegetales fósiles del complejo Cerro Guido-Las Chinas: cambios en la composición florística y fisionomía foliar asociados al enfriamiento del Cretácico Superior. 1er Congreso Chileno de Paleontología, Libro de Resúmenes, pp. 238-241.

Plink-Björklund, P., Hampson, G. J., Steel, R. J., Burgess, P. M., & Dalrymple, R. W. (2008). Wave-to-tide facies change in a Campanian shoreline complex, Chimney Rock Tongue, Wyoming-Utah, USA. *Recent advances in models of shallow-marine stratigraphy: SEPM Special Publication*, *90*, 265-291.

Povilauskas, L. (2017). Palynostratigraphy of the Cretaceous–Paleogene in the Austral basin, SW Santa Cruz Province, Argentina. *Revista Brasileira de Paleontologia*, *20*(3), 299-320. doi:10.4072/rbp.2017.3.03

Reinson, G. E. (1992). Transgressive barrier island and estuarine systems. In R.G., Walker, & N.P., James (Eds.), Facies Models: Response to Sea Level Changes (pp. 179-194). St. Johns, Newfoundland & Labrador: Geological Association of Canada.

Rivera, H. A. (2017). Insights into the tectonostratigraphic evolution of the Southern Magallanes Basin, Southern Chile, during the Cenozoic. (Master's thesis) Universidad de Chile, Santiago, Chile, 149 pp. Available from http://repositorio.uchile.cl/handle/2250/146413

Rivera, H. A., Le Roux, J. P., Sánchez, L. K., Mariño-Martínez, J. E., Salazar, C., & Barragán, J. C. (2018). Palaeoredox conditions and sequence stratigraphy of the Cretaceous storm-dominated, mixed siliciclastic-carbonate ramp in the Eastern Cordillera Basin (Colombia):

Evidence from sedimentary geochemical proxies and facies analysis. *Sedimentary geology*, *372*, 1-24. https://doi.org/10.1016/j.sedgeo.2018.05.003

Roddaz, M., Hermoza, W., Mora, A., Baby, P., Parra, M., Christophoul, F., ... & Espurt, N. (2010). Cenozoic sedimentary evolution of the Amazonian foreland basin system. *Amazonia, landscape and species evolution: a look into the past. Blackwell-Wiley, Hoboken*, 61-88. https://doi.org/10.1002/9781444306408.ch5

Romans, B. W., Fildani, A., Graham, S. A., Hubbard, S. M., & Covault, J. A. (2010). Importance of predecessor basin history on the sedimentary fill of a retroarc foreland basin: provenance analysis of the Cretaceous Magallanes basin, Chile (50-52 S). *Basin Research*, *22*(5), 640-658. https://doi.org/10.1111/j.1365-2117.2009.00443.x

Rossi, V. M., & Steel, R. J. (2016). The role of tidal, wave and river currents in the evolution of mixed-energy deltas: Example from the Lajas Formation (Argentina). *Sedimentology*, *63*(4), 824-864. https://doi.org/10.1111/sed.12240

Sánchez, A. (2006). Proveniencia sedimentaria de estratos de Cabo Naríz y Formación Cerro Toro, Cretácico Tardío-Paleoceno, Magallanes, Chile. (Master's thesis), Universidad de Chile, Santiago, Chile, 153 pp.

Sánchez, A., Pavlishina, P., Godoy, E., Herve, F., & Fanning, C. M. (2010). On the presence of Upper Paleocene rocks in the foreland succession at Cabo Nariz, Tierra del Fuego, Chile: geology and new palynological and U-Pb data. *Andean Geology*, *37*(2), 413-432.

Schwartz, T. M., & Graham, S. A. (2015). Stratigraphic architecture of a tide-influenced shelf-edge delta, Upper Cretaceous Dorotea Formation, Magallanes-Austral Basin, Patagonia. *Sedimentology*, *62*(4), 1039-1077. https://doi.org/10.1111/sed.12176

Schwartz, T. M., Fosdick, J. C., & Graham, S. A. (2017). Using detrital zircon U-Pb ages to calculate Late Cretaceous sedimentation rates in the Magallanes-Austral basin, Patagonia. *Basin Research*, *29*(6), 725-746. https://doi.org/10.1111/bre.12198

Sial, A. N., Ferreira, V. P., Toselli, A. J., Parada, M. A., Acenolaza, F. G., Pimentel, M. M., & Alonso, R. N. (2001). Carbon and oxygen isotope compositions of some Upper Cretaceous–Paleocene sequences in Argentina and Chile. *International Geology Review*, *43*(10), 892-909. https://doi.org/10.1080/00206810109465054

Sinclair, H. D., Sayer, Z. R., & Tucker, M. E. (1998). Carbonate sedimentation during early foreland basin subsidence: the Eocene succession of the French Alps. *Geological Society, London, Special Publications*, *149*, 205-227. https://doi.org/10.1144/GSL.SP.1999.149.01.11

Vellekoop, J., Holwerda, F., Prámparo, M. B., Willmott, V., Schouten, S., Cúneo, N. R., ... & Brinkhuis, H. (2017). Climate and sea-level changes across a shallow marine Cretaceous–Palaeogene boundary succession in Patagonia, Argentina. *Palaeontology*, *60*(4), 519-534. https://doi.org/10.1111/pala.12297

Yang, Y., & Miall, A. D. (2008). Marine transgressions in the mid-Cretaceous of the Cordilleran foreland basin re-interpreted as orogenic unloading deposits. *Bulletin of Canadian Petroleum Geology*, *56*, 179-198. https://doi.org/10.2113/gscpgbull.56.3.179

Zaitlin, B. A., Dalrymple, R. W., & Boyd, R. O. N. (1994). The stratigraphic organization of incised-valley systems associated with relative sea-level change. In: R.W. Dalrymple, R.J. Boyd & B.A. Zaitlin (Eds.), Incised valley systems: Origin and sedimentary Sequences (pp. 45-60). SEPM Special Publications 51.

TABLE CAPTIONS

Table 1. List of measured stratigraphic sections, and units studied, also geographic distribution along the basin strike. For geographical location, see Fig. 2.

Table 2. Characteristic facies and interpreted sedimentary processes of the K-Pg units in the Magallanes-Austral Basin. BI=bioturbation index.

Table 3. Summary of palynomorph taxa recorded in the Rocallosa Formation with their botanical affinity and palaeoclimatic significance. CT= cool temperate (6-12°C), WT= warm temperate (12-17°C).

APPENDICES

Appendix S1. Detailed mineral separation technique, and analytical procedures of detrital zircon U-Pb geochronology and maximum depositional age calculation.

Appendix S2. Detrital zircon U-Pb geochronological analyses by using LA-ICP-MS and LA-MC-ICP-MS.

Appendix S3. Probability density plots and Wetherill Concordia diagrams of the samples. (a) Sample RB1. (b) Sample PB1. (c) Sample ZPR1. (d) Sample ZLP1.

Appendix S4. Point-count raw data and equations for recalculated Q-F-L, and Qm-F-Lt plots.

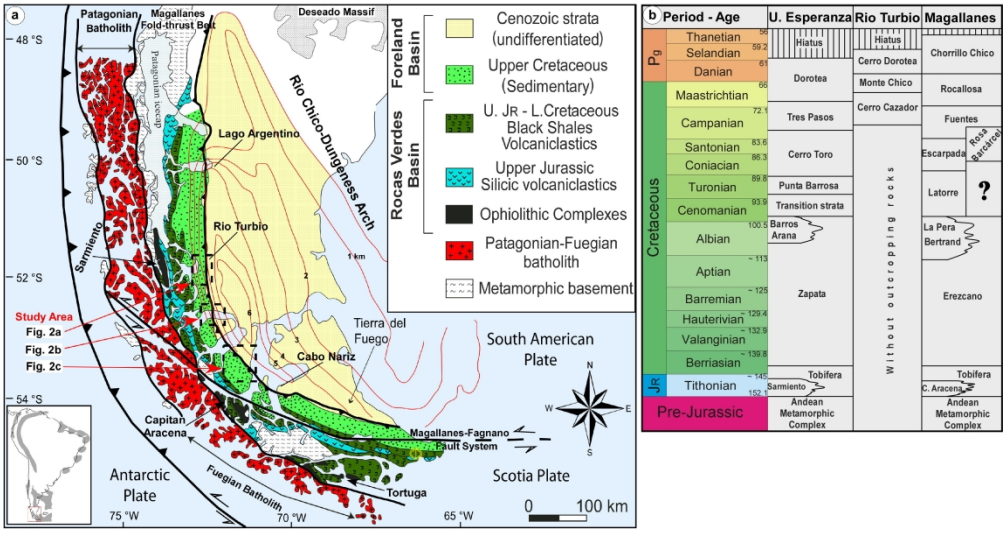

Figure 1. (a) Simplified morphotectonic map of the Magallanes-Austral Basin (modified from Fildani et al., 2008), showing the location of the study area and other locations mentioned in the text. The inset map shows the distribution of the Maastrichtian-Danian transgression in South America. (b) Correlation chart of stratigraphic units studied, highlighting different nomenclatures used in adjacent areas within the basin.

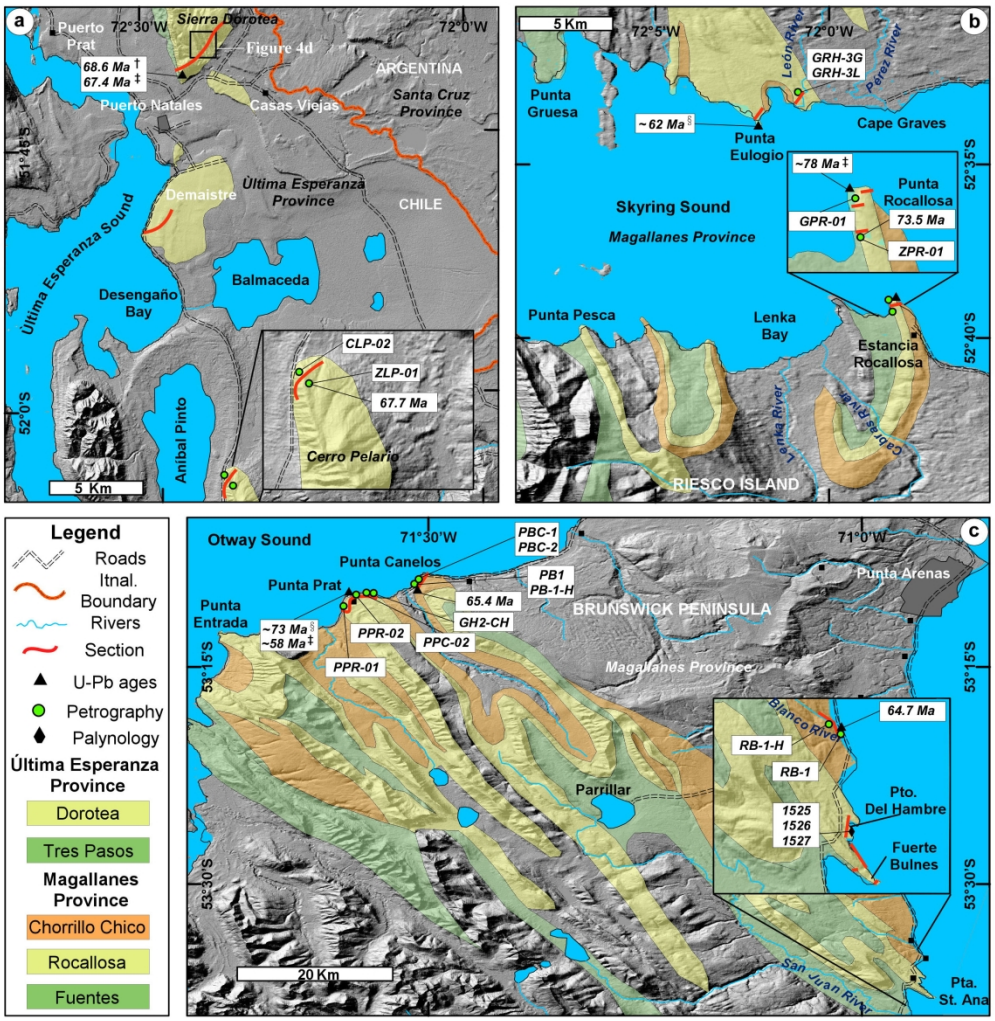

Figure 2. Geographical distribution of geological units, sections, and samples in the Última Esperanza Province (UEP) (a), Skyring sound (b), and Brunswick Peninsula areas (c) within the Magallanes Province (MP). † Fosdick et al., 2015 ‡ Hervé et al., 2004.

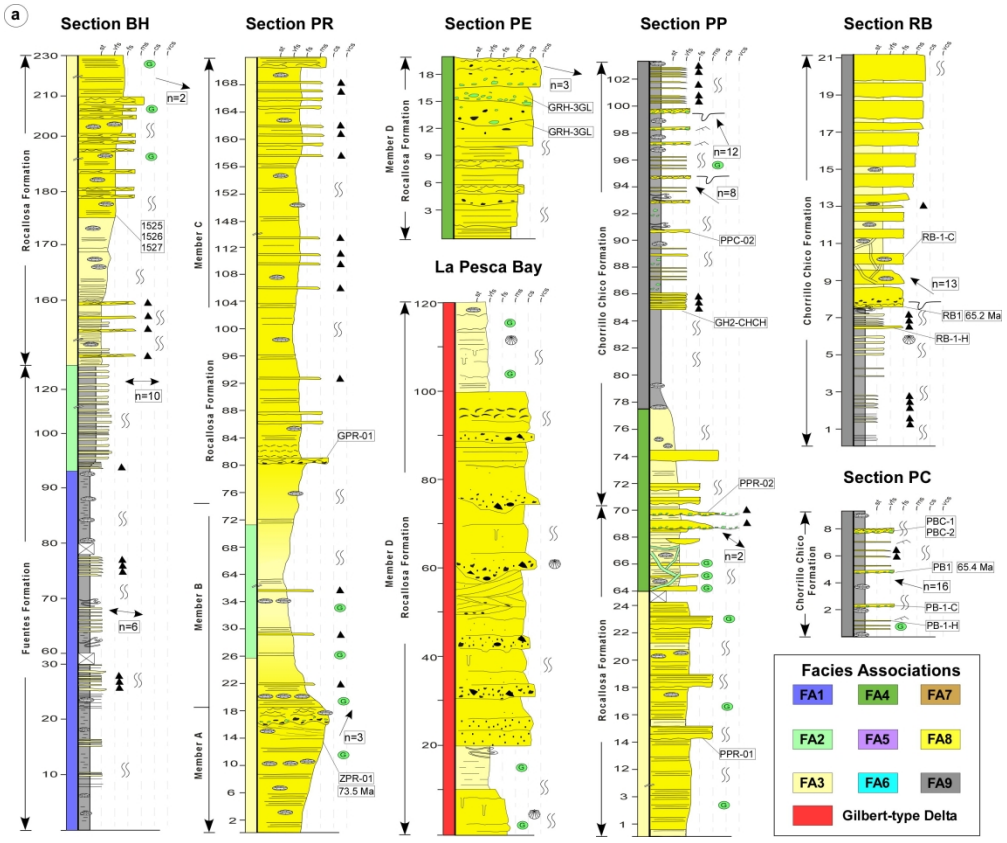

Figure 3. Stratigraphic profiles illustrating facies associations, palaeocurrents, and sampled intervals. (a) Stratigraphic columns of the Fuentes, Rocallosa, and Chorrillo Chico Formations in the MP. (b) Stratigraphic columns of the Dorotea Formation in the UEP. For location, see Fig. 2.

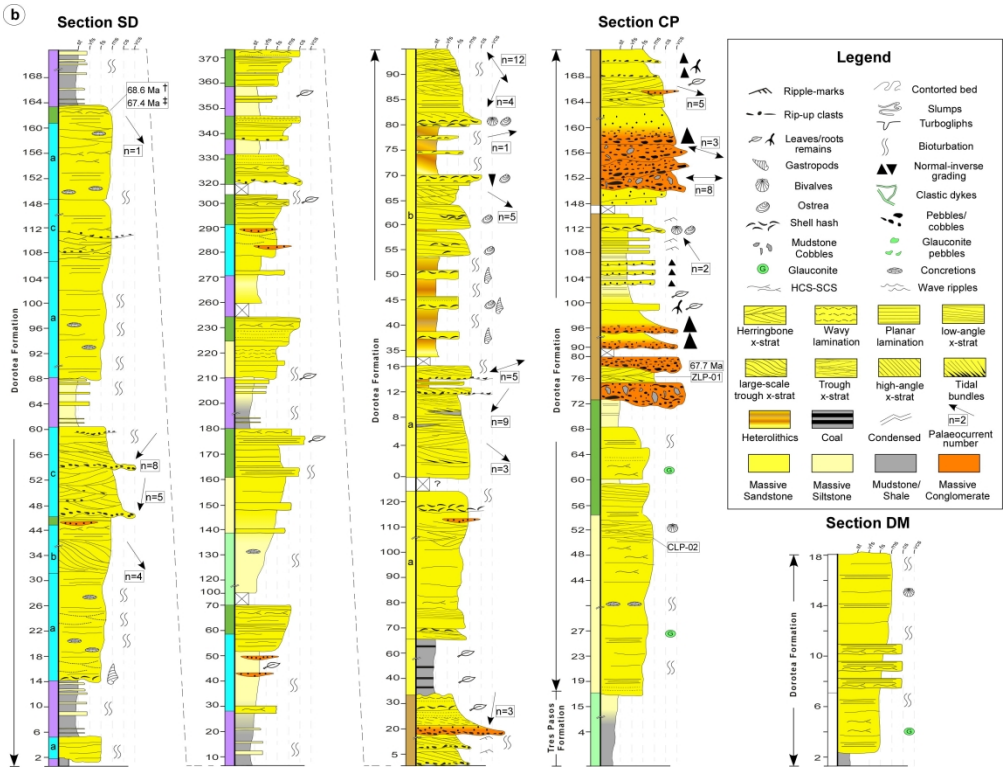

Figure 3. Stratigraphic profiles illustrating facies associations, palaeocurrents, and sampled intervals. (a) Stratigraphic columns of the Fuentes, Rocallosa, and Chorrillo Chico Formations in the MP. (b) Stratigraphic columns of the Dorotea Formation in the UEP. For location, see Fig. 2.

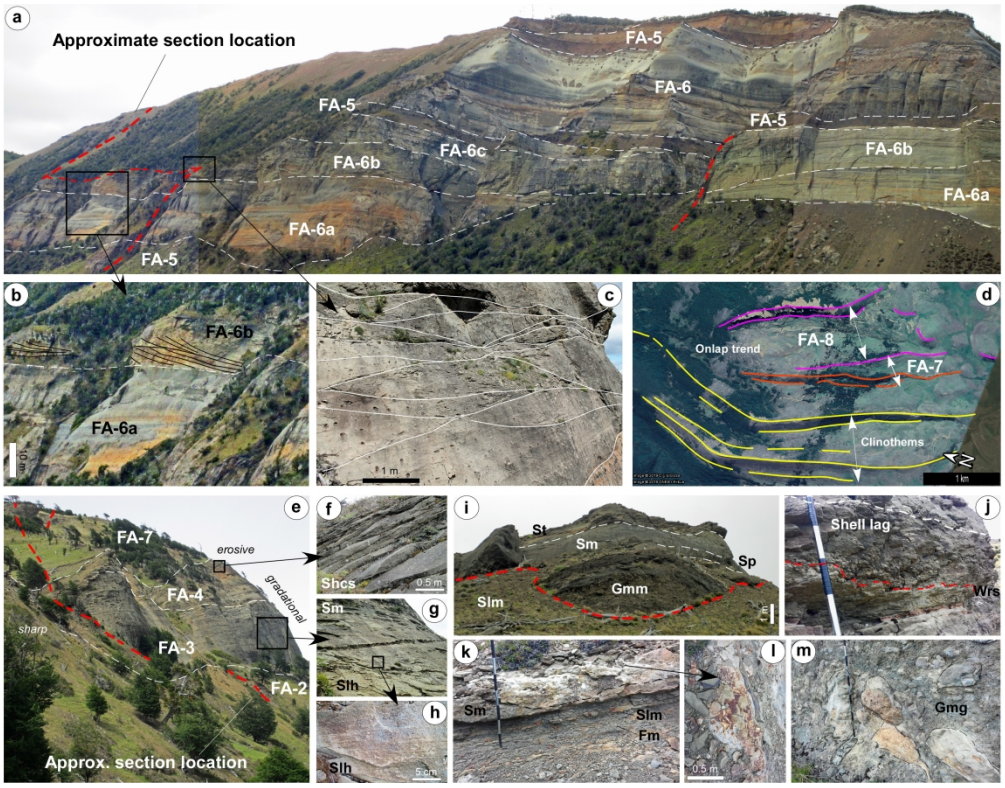

Figure 4. (a) Overview (view to NE) of facies associations interpreted for the Dorotea Formation in the basal part of section SD. (b) Example of large-scale foresets of trough cross-stratification of the FA6b. (c) Amalgamated channel of FA6b displaying internal planar lamination (Spl) and hummocky, and swaley cross-lamination (Shcs) locally. (d) Google Earth plane-view of clinothems of the Dorotea Formation and onlap trend of the FA8 over the FA7. (e) Overview (view to S) of facies associations interpreted for the Dorotea Formation in the section CP. (f) Amalgamated beds of hummocky and swaley cross-stratification (Shcs). (g) Outcrop expression of FA3. (h) Subtle planar lamination in siltstones of the FA3. (i) Distribution of facies within encased channel body (FA7) of the incised valley system in section CP. (j) Example of shell lag and wave ravinement surface on the fluvial channels marking the start of TST in section CP. (k) Overbank deposits and development of palaeosols. (l) Plane view of iron oxide nodules and root remains in pedogenetic layer, section CP. (m) Example of mudstone/sandstone blocks in fluvial facies. Jacob staff divisions each 10 cm.

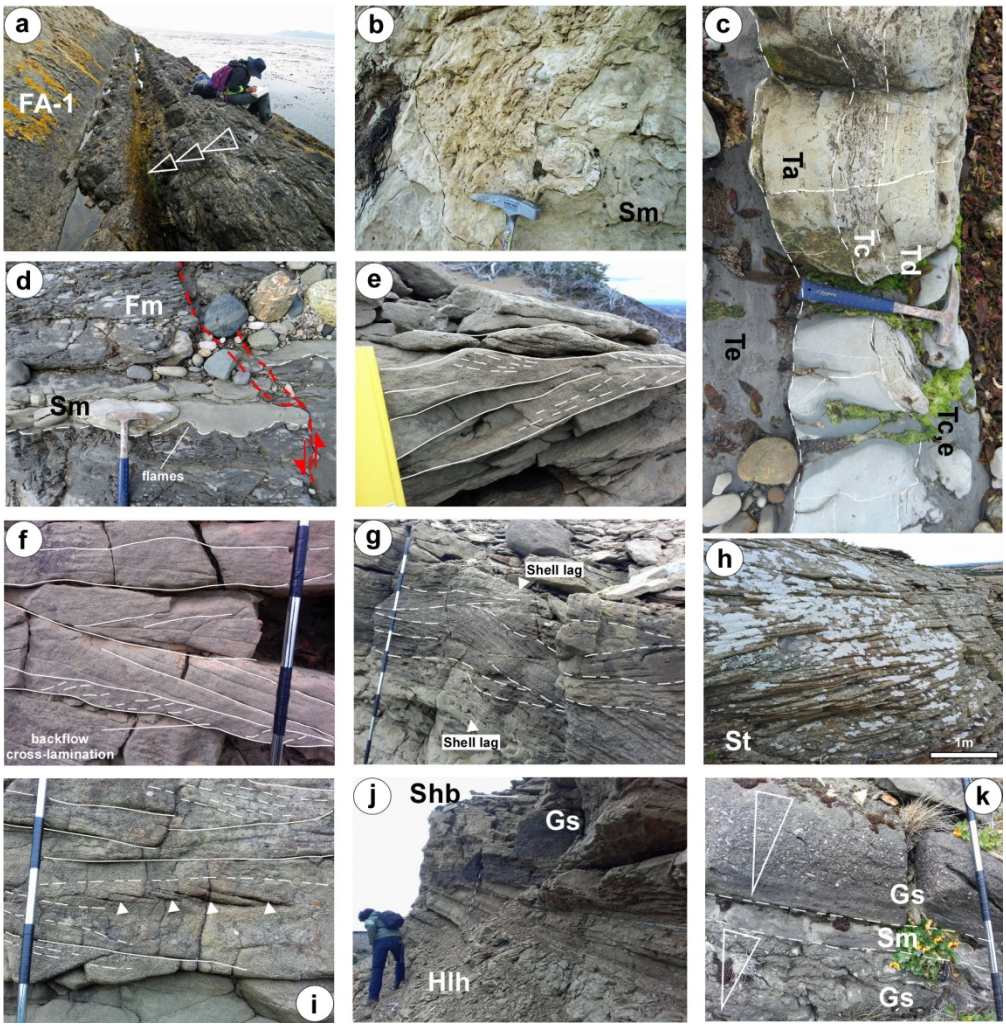

Figure 5. (a) Outcrop expression (view to SE) of the FA1, note normal graded beds representing distal turbidite currents in the uppermost Fuentes Formation (section BH). (b) Plan view of contorted bedding in the Chorrillo Chico Formation in section RB. (c) Bouma sequence in turbidite deposits of the FA9. (d) Loading structures in lobe fringe deposits (FA9) in section PP. (e-g) Herringbone and bidirectional cross-stratification in estuary deposits (FA8) in upper part of section SD. (h) Washed-out 3D megaripples in estuary mouth complex (FA8a; spit platform). (i) Example of large-scale, low-angle inclined heterolithic units (Hlh) overlying by tidal creeks channels in the FA8b. (k) Inverse grading of shelly sandstones and conglomerates reflecting turbulent currents of fluvial origin in the FA8b. Jacob staff divisions each 10 cm.

Figure 6. Selected ichnofossils of the studied succession. (a) Phycodes isp., in the FA1. (b) *Neonereites* isp., of the FA9. (c) *Scolicia* (*Laminites*) of the FA9. (d) *Phoebichnus bosoensis* in the FA1. (e) *Cladichnus* cf. *fischeri* of the FA1. (f) *Stelloglyphus llicoensis* in FA1. (g) *Rhizocorallium* isp., in the FA9. (h) Assemblage of *Chondrites* isp., *Planolites* isp., *Zoophycos* isp., and *Teichichnus* isp. in the FA2. (i) *Macaronichnus* isp. of the FA6. (j) *Teichichnus* isp., and *Chondrites* isp., in the FA3. (k) *Schaubcylindrichnus* isp., of the FA6. (l) *Skolithos* isp. suite of the FA8.

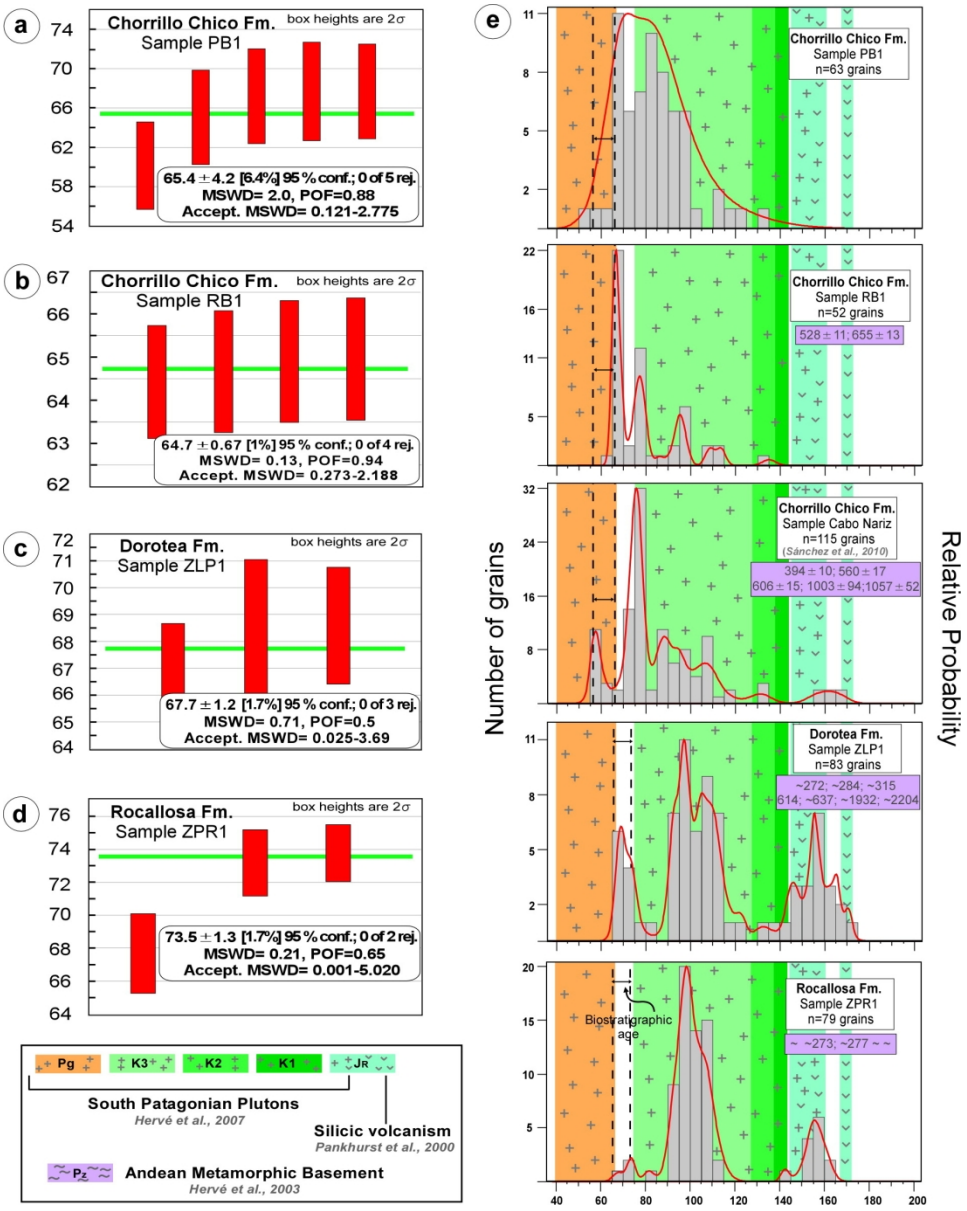

Figure 7. Maximum depositional age interpretations from YP-WMA from the Chorrillo Chico Formation samples (a, b), Dorotea Formation sample (c) and from the Rocallosa Formation sample (d). (e) Composite histograms and probability plots for DZ U-Pb age populations from the Rocallosa, Cabo Nariz beds (Sánchez et al., 2010), and Chorrillo Chico Formations. Lower case "n" below the sample name refers to total number of grains younger than 200 Ma. Grains > 200 Ma are indicated in the lower violet box. Potential source terranes are indicated in the inset box.

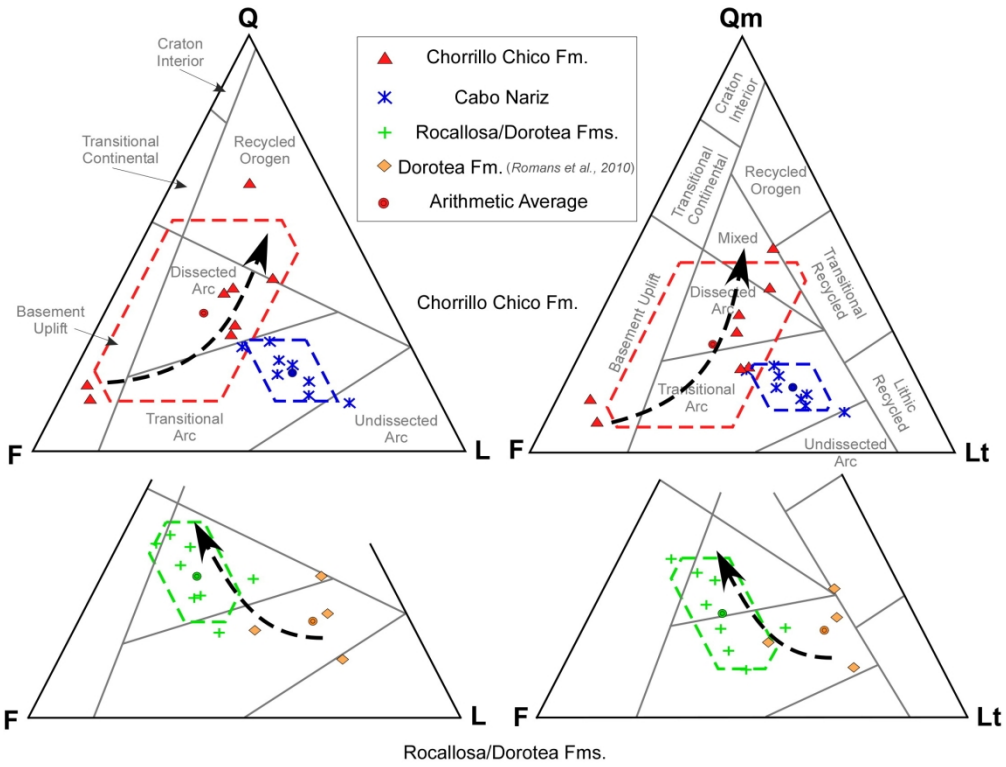

Figure 8. Q-F-L and Qm-F-Lt ternary plots displaying detrital modes for the Rocallosa-Dorotea, Cabo Nariz, and Chorrillo Chico Formations. Tectonic provenance fields from Dickinson (1985); polygons represent univariate confidence intervals. Note the unroofing trend in the Chorrillo Chico Formation and between the Dorotea (northern samples of Romans et al., 2010), and Dorotea-Rocallosa Formations (southern samples of this study).

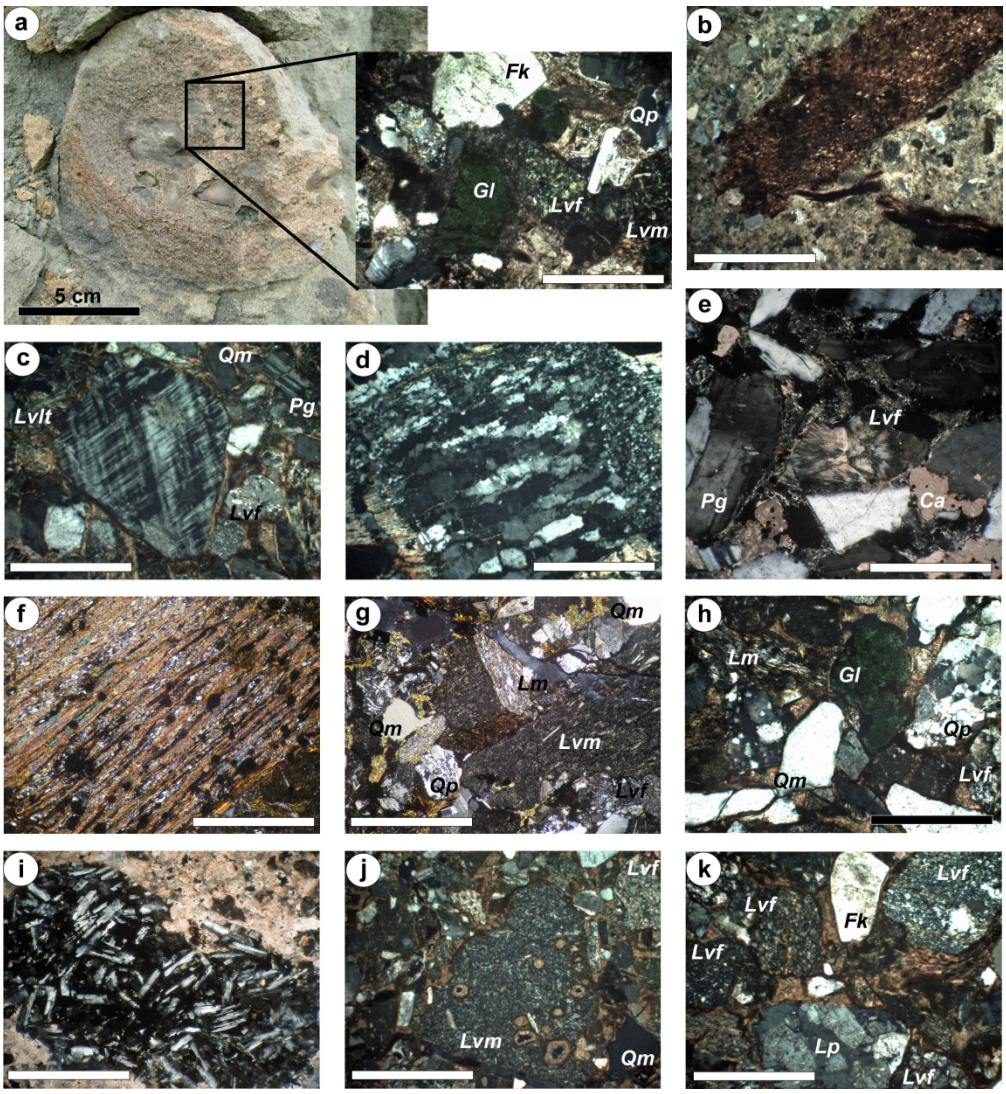

Figure 9. (a) Cobble of Member D of the Rocallosa Formation showing (inset) abundant reworked glauconite (Gl) grains, volcanic lithics, and altered K-feldspar (Fk). (b) Plant remains of the Chorrillo Chico Formation. (c) Microcline grain with exsolution textures typical of the Rocallosa-Dorotea Formations. (d) Metamorphic lithic fragment of the Rocallosa Formation. (e) Devitrified felsitic volcanic lithic in the Chorrillo Chico Formation, suggesting input from the Tobífera Formation. (f) Micaceous schist lithic fragment representative of the Rocallosa-Dorotea Formations and Cabo Nariz beds. (g) Microlitic (Lvm) and felsitic (Lvf) textures in volcanic lithic fragments of the Cabo Nariz beds. (h) Abundant polycrystalline quartz (Qp), felsitic (Lvf) volcanic lithic, metamorphic lithic (Lm) grains in the Dorotea Formation. Note siliceous protolith of the metamorphic lithic fragments. (i) Lathwork texture (Lvlt) of volcanic lithic in the Chorrillo Chico Formation, suggesting the input of mafic rocks. (j) Example of microlitic (Lvm) texture with palagonite filling (partly) vesicles of a basalt fragment in the Rocallosa Formation. (k) Abundant felsitic (Lvf) volcanic lithic and some plutonic lithic fragment (Lp) typical of the Rocallosa and Chorrillo Chico Formations.

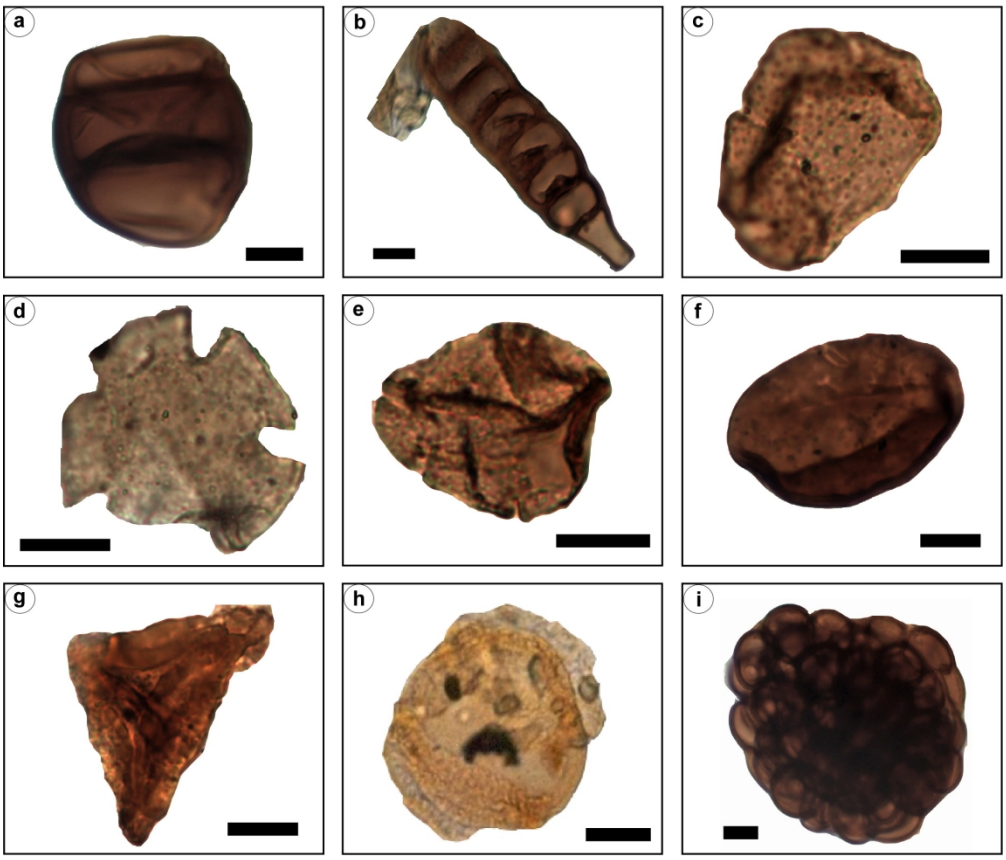

Figure 10. Light transmitted images of selected terrestrial palynomorph specimens from the Rocallosa Formation. (a) *Granatisporites* sp. (b) *Multicellaesporites* sp. (c) *Nothofagidites brassii* type. (d) *Nothofagidites dorotensis*. (e) *Nothofagidites cincta*. (f) *Laevigatosporites vulgaris*. (g) *Clavifera triplex*. (h) *Podocarpidites otagoensis*. (i) *Botryococcus braunii*. Scale is 10 μm.

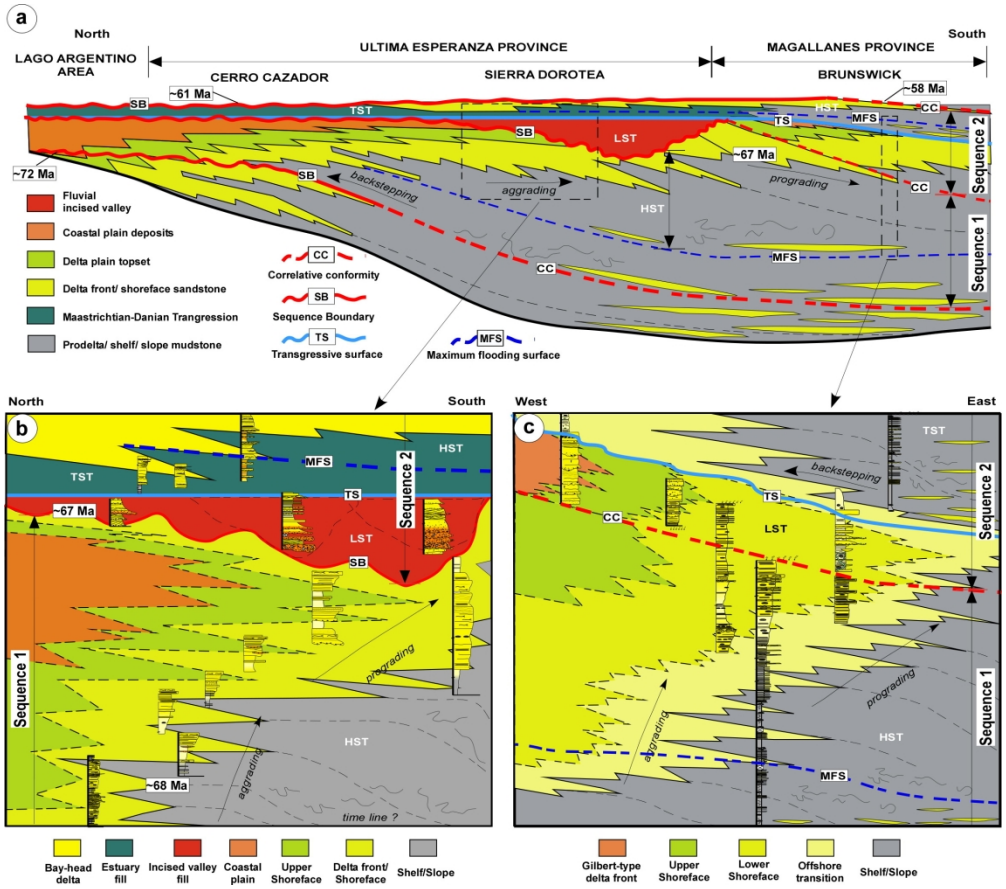

Figure 11. (a) Idealized sequence stratigraphic model along-strike the Magallanes Basin. Note how the development of the sequence boundaries and correlative conformities depends upon the basin palaeo-bathymetry. (b) Sequence stratigraphic framework interpreted for the uppermost Tres Pasos-Dorotea Formations in the UEP (b) and for the uppermost Fuentes, Rocallosa, and Chorrillo Chico Formation in the MP (c). LST=lowstand system tract; HST=highstand system tract; TST=transgressive system tract.

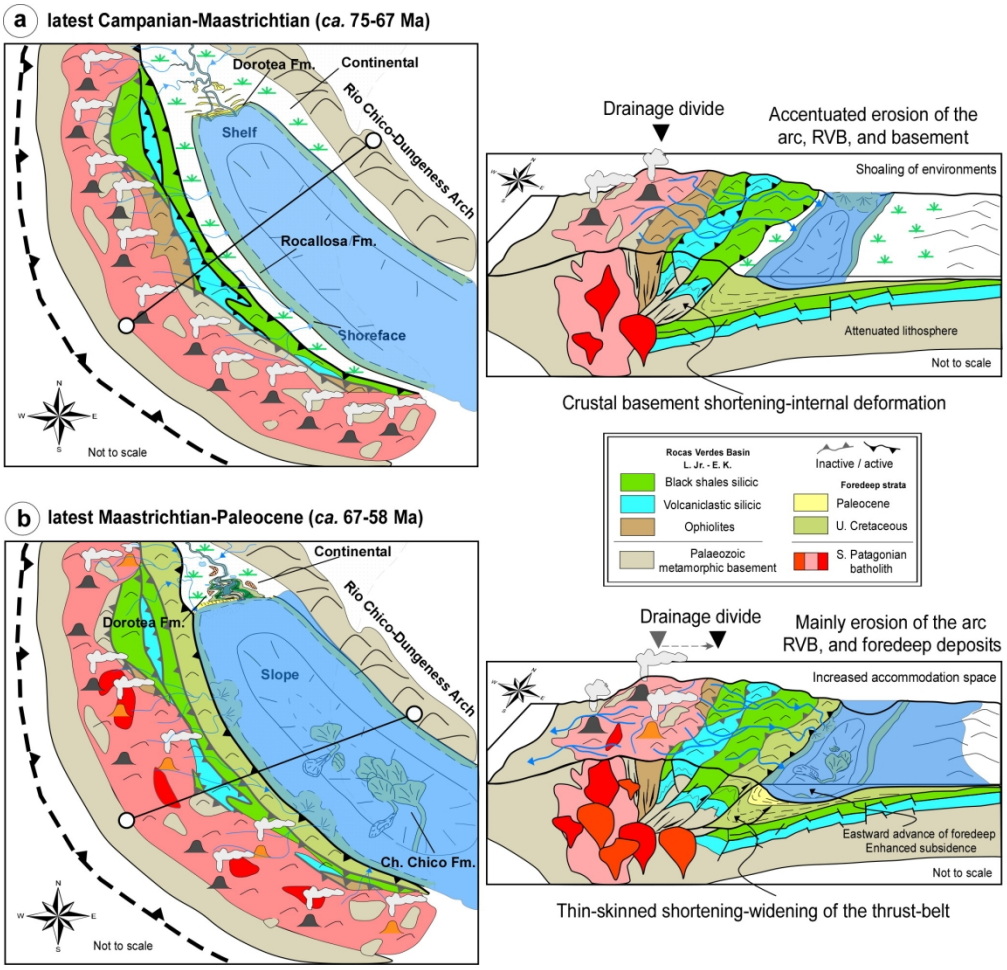

Figure 12. Simplified palaeogeographic/palaeotectonic reconstruction and schematic structural configuration of the Patagonian thrust-belt and Magallanes-Austral foredeep before (a), and after (b) of the occurrence of the first Atlantic marine transgression. Note that palaeogeographic maps are not palinspastically restored and diagrams not to scale.

Section Name	Abbreviated Name	Formation studied	Location
Sierra Dorotea	**SD**	Dorotea	Última Esperanza Province
Demaistre	**DM**		
Cerro Pelario	**CP**		
Punta Eulogio	**PE**	Rocallosa	Magallanes Province
Punta Rocallosa	**PR**		
Punta Canelos	**PC**	Chorrillo Chico	
Punta Prat	**PP**	Rocallosa-Chorrillo Chico	
Fuerte Bulnes-Puerto del Hambre	**BH**	Rocallosa	
Río Blanco	**RB**	Chorrillo Chico	

Code	Lithology	Sedimentary structures	Geometry–contacts–thickness	Fossils – Bioturbation	Sedimentary processes
Fh	Light- to greenish-gray shales and silty shales; carbonaceous or coaly paper shales	Finely laminated to fissile; internally with normal grading from silt-grade material to laminated shales; slump and contorted bedding	Tabular – Sharp, planar to undulate (wavy) contacts – 15cm up to 1m	Scarce fossils; (BI=0-2) *Chondrites* isp., *Phycosiphon incertum ?, Planolites* isp., and rarerly *Bergaueria* isp., *Zoophycus* isp.	Deposition by suspension and vertical settling in very low- to moderated-energy and poorly-oxygenated environments below of the storm-wave base level; or in quiet, low-energy environments with abundant organic material supply and undisturbed by current energy.
Fm	Light-black to grayish mudstones	Massive to hardly laminated	Tabular – sharp and planar contacts – up to 10's m	Scarce fossils; (BI=2-3) *Phycodes* isp., *Stelloglyphus llicoensis, Palaeophycos* isp., *Cladichnus* cf. *fischeri,* and *Phoebichnus bosoensis, Planolites* isp., *Taenidium* isp., *Chondrites* isp.	Deposition by suspension and fast vertical settling in very low- to moderated-energy below of the storm-wave base level. In some cases, structureless appearance can be by bioturbation
Slm	Tan, and grayish siltstones, and lower very fine-grained sandstone	Massive to poorly laminated ; internally normal grading	Tabular – Sharp-gradual, planar to undulate (wavy) contacts – 15cm up to 90 cm	Null fossils; (BI=0-1) *Cylindrichnus* isp., horizontal and vertical unidentified trace fossils	Sedimentation by fast vertical settling in low- to moderated-energy environments
Slh	Beige to pale yellow, buff (weathered) siltstones	Parallel laminated, wispy lamination	Tabular – Sharp, planar to undulate (wavy) contacts – 15 to 50 cm, up to 1m	Null fossils; (BI=0-1) horizontal and vertical unidentified trace fossils	Sedimentation by suspension and vertical settling in low- to moderated-energy environments with alternating low and moderate current intensity on the sea floor
Hlh	Rhythmic intercalations of pale siltstones and very fine-grained sandstones and reddish mudstones	Horizontal to low-angle laminated, tidal rythmites ; lenticular bedding	Tabular– sharp contacts—bedsets of up to 3m	Pervasive bioturbation (BI=4-5)	Fluctuations in in strength, and suspended sediment supply likely reflecting seasonally or climatic controls, typically associated with a tidal regime
Sm	Tan, whitish to green, and grayish very fine-to-very coarse-grained (glauconitic or shelly) sandstones	Massive or crudely graded; amalgamated; poorly bedded	Sub-tabular to tabular, lenticular–sharp and planar contacts, or erosive base–10cm up to 10's m	Lenticular bodies with highly fragmented bivalves, gastropods, and oysters. Shell, pebble or mudstone lag deposits on erosional contacts; (BI=0-5) *Thalassinoides* isp., *Cylindrichnus* isp., horizontal unidentified trace fossils	Rapid accumulation of sand from sediment gravity flows or under conditions of rapid flows carpet shear (fraction- carpet); fast accumulation of sand and shells in channels by high-energy events. Structureless appearance also can be relate to bioturbation
Sw	Beige, buff (weathered) fine-to-medium-grained sandstones	Symmetrical and asymmetrical wave ripples, undulate lamination; slightly contorted lamination	Tabular–sharp and planar base, rippled top surface –30cm up to 50cm	Null fossils; (BI=0-2) horizontal and vertical unidentified trace fossils	Oscillatory flows and combined flows in shallow waters with bottom friction; alternating traction currents in lower flow regime with vertical accretion processes

Sr	Pale yellow, light gray very fine-to-fine-grained sandstone	Current ripples	Tabular– sharp contacts– 30cm up to 1m	Null fossils; in a few cases mottled (BI=4-6).	Sedimentation of migrating bedforms under unidirectional currents and lower flow regime
Shcs	Fine-to-medium-grained sandstones; commonly with pebble lag	Amalgamated or isolated hummocky, and swaley cross-stratification/lamination	Tabular, amalgamated–sharp or erosive base and gradual top–20cm up to 60 cm	Null fossils, plant or carbonaceous debris; (BI=0-1).	Deposition by combined oscillatory and unidirectional currents well above storm wave-base and near fair-weather wave-base
Spl	Gray to greenish, fine-to-medium-grained sandstones	Lower or upper planar lamination; low-angle cross-lamination; well bedded	Tabular–sharp to gradual base– 20cm to 1m	Null large fossils, plant or carbonaceous debris; (BI=0-2), *Skolithos* isp.,	Sedimentation from suspension in calm water or under supercritical flow conditions; related to sedimentation on the surf or swash zone of beaches
Spa	Whitish, medium-to-coarse-grained sandstone	High-angle, planar cross-stratification; crude to well bedded	Sub-tabular–sharp and scoured bases– 2 up to 4m	Null fossils; (BI=0-1), *Schacylindrichnus* isp	Related to migration of straight-crested (2D) dunes or sand waves, and scroll bars.
St	Gray to greenish, fine-to-medium-grained sandstones	Trough cross-lamination; medium-to-large-scale trough cross bedding; tangential-based cross lamination with mud drapes.	Sub-tabular–sharp and planar contacts– 50 cm up to 4 m	Some *Turritela* sp. and fragmented shells; (BI=1-2), *Macaronichnus* isp., *Planolites* isp., *Diplocraterion* ? isp	Related to migrating lunate or sinuous (3D) subaqueous dunes or wind dunes, modified by tides forming epsilon cross bedding. Large-scale migrating dunes are linked to prograding clinoforms.
Shb	Tan, fine- to medium-grained sandstones	Bidirectional cross-bedding ; herringbone cross-lamination; mud-drapes, and partings	Tabular–sharp contacts–30 to 90cm	Null fossils and bioturbation absent. Shell hash common.	Migrating 2D-3D dunes products of high-energy ebb and flood currents, whereas the mud represents irrupting slackwater stages.
Gmm	Grayish to pale, (sub-) angular to sub-rounded pebbly to cobble conglomerates	Sandy matrix-supported, structureless; large clasts up to 1m long	Lenticular, tabular–sharp, erosive bases– 1up to11 m (amalgamated)	Shell hash, carbonaceous fragments, bioturbation absent.	Cohesive debris flow, hyperconcentrated sheet flood, generally high-shear strength preventing turbulence
Gmg	Grayish to light brown, sub-angular to rounded coarse to fine pebbly conglomerates	Sandy clast- to matrix-supported, massive to normal grading, rare inverse grading.	Lenticular to subtabular– sharp, scoured bases; gradational top– up to 5 m	Null fossils, carbonaceous fragments, bioturbation absent.	Winnowing of finer sediments forming a lag. Bed-load deposition from somewhat diluted turbulent stream flows. Inverse grading related to dispersive pressure on density-grain flows.
Gs	Grayish to dark-gray coarse shelly conglomerates	Clast-(shell-)supported, normal grading in shells; often massive	Tabular to subtabular, lenticular– sharp contacts– up to 2m	Oysters, bivalves, *Turritella* isp. and very fragmented shells; bioturbation absent	Basal lag or shelly debris product of high-energy erosion and redeposition

Palynomorphs	Taxa	Botanical affinity	Climate type
Epiphytic fungi (40.9%)	*Granatisporites* sp. (Fig. 10a)	Uncertain	–
	Multicellaesporites sp. (Fig. 10b)	Meliolaceae	
	Monoporisporites sp.		
Magnoliophyta (27.7%)	*Nothofagidites brassii* type (Fig. 10c)	Dicotyledonae, Nothofagaceae, *Nothofagus* *Nothofagus betuloides*	CT
	N. dorotensis (Fig. 10d)		
	N. cincta (Fig. 10e)		
	N. diminuta		
	N. flemingii		
	N. spinosus		
	Gaultheria sp.	Dicotyledoneae	WT
	Tricolpites sp.		
	Monocoplites sp.$^{\psi}$	Monocotyledoneae	
Pteridophyta (21.4%)	*Laevigatosporites vulgaris* (Fig. 10f)	Filicopsida, ?Blechnaceae	WT
	Cyathidites minor	Filicopsida, Cyatheaceae	
	Gleicheniidites sp.	Filicopsida, Gleicheniaceae	
	G. senonicus	*Gleichenia circinata*	
	Clavifera triplex (Fig. 10g)	*Dicranopteris rigida*	
	Lycopodium austroclavidites	Lycopodiaceae, *Lycopodium*	
	Polypodiisporites sp.	Uncertain	
Pinophyta (7%)	*Podocarpidites otagoensis* (Fig. 10h)	Podocarpaceae, *Podocarpus* *Podocarpus salignus*	CT
	P. marwickii		
	Araucariacites australis	Araucariaceae (*Araucaria*)	
Microalgae colonies (3%)	*Botryococcus braunii* (Fig. 10i)	Chlorophyta, Chlorococcales, Botryococcaceae	–
Minor dinocysts	*Spiniferites* sp.	Dinoflagellata	–

$^{\psi}$ Representing 10.2% from the overall Magnoliophytas identified; CT=cool temperate; WT=warm temperate